REPORT DOCUMENTATION PAGE

1. REPORT DATE	2. REPORT TYPE	3. DATES COVERED	
		START DATE	END DATE
20240427	Final	Oct. 15, 2020	Jan. 14, 2024

4. TITLE AND SUBTITLE

NEMO Data Analysis and Environmental System Data Collection in Alternate Location Plan

5a. CONTRACT NUMBER	5b. GRANT NUMBER	5c. PROGRAM ELEMENT NUMBER
	N00014-21-1-4007	
5d. PROJECT NUMBER	**5e. TASK NUMBER**	**5f. WORK UNIT NUMBER**

6. AUTHOR(S)

Soloviev, Alexander. V.

7. PERFORMING ORGANIZATION NAME(S) AND ADDRESS(ES)
Nova Southeastern University
3301 College Ave, Fort Lauderdale, FL 33314

8. PERFORMING ORGANIZATION REPORT NUMBER

9. SPONSORING/MONITORING AGENCY NAME(S) AND ADDRESS(ES)	10. SPONSOR/MONITOR'S ACRONYM(S)	11. SPONSOR/MONITOR'S REPORT NUMBER(S)
Office of Naval Research	ONR	

12. DISTRIBUTION/AVAILABILITY STATEMENT
Approved for public release; distribution unlimited.

13. SUPPLEMENTARY NOTES

14. ABSTRACT

. The goal of this project is to support the development and validation of the electromagnetic (EM) model of internal waves (IWs) at Navy Electromagnetic Observatory (NEMO) in the Straits of Florida and planning the model assessment in alternate ocean environmental conditions.

Respectively, our specific scientific objectives are as follows:

- Verify the EM model with data from NEMO
- Identify suitable locations and plan deployment of the portable environmental data collection system, developed on a previous project, for the purpose of electromagnetic model validation in alternate environmental conditions.

In this project, the Navy and NSU have worked together to identify suitable alternate locations to deploy the portable environmental data collection system. The results of this investigation suggested that at the Alaska location the signature of high-frequency IWs to be measured by bottom-based magnetometers may be too close to the noise level of even very sensitive magnetometers. This is the main challenge for conducting the IW magnetic signature experiment at the location in Alaska. Assessments of potential sites have been discussed with the Navy. After consulting with our Navy partners, the final location for an alternative environment internal wave experiment was selected in Scotland, UK

The anticipated outcome of the research is an advanced MHD model verified in the western boundary current (Florida Current) and at an alternate location with different environmental conditions. Potential applications of the results of this study for DoD include locating underwater vehicles from aircraft. Other applications involve geophysical prospecting for oil and minerals under the seafloor and for archeological investigations, and environmental assessment studies.

15. SUBJECT TERMS				
Straits of Florida, Southern California, Alaska, Scotland, ocean circulation, internal waves, CFD, MHD, numerical modeling, air-sea interaction				
16. SECURITY CLASSIFICATION OF:			**17. LIMITATION OF ABSTRACT**	**18. NUMBER OF PAGES**
a. REPORT	**b. ABSTRACT**	**C. THIS PAGE**		
U	U	U	UU	

19a. NAME OF RESPONSIBLE PERSON	19b. PHONE NUMBER *(Include area code)*

INSTRUCTIONS FOR COMPLETING SF 298

1. REPORT DATE.
Full publication date, including day, month, if available. Must cite at least the year and be Year 2000 compliant, e.g. 30-06-1998; xx-06-1998; xx-xx-1998.

2. REPORT TYPE.
State the type of report, such as final, technical, interim, memorandum, master's thesis, progress, quarterly, research, special, group study, etc.

3. DATES COVERED.
Indicate the time during which the work was performed and the report was written.

4. TITLE.
Enter title and subtitle with volume number and part number, if applicable. On classified documents, enter the title classification in parentheses.

5a. CONTRACT NUMBER.
Enter all contract numbers as they appear in the report, e.g. F33615-86-C-5169.

5b. GRANT NUMBER.
Enter all grant numbers as they appear in the report, e.g. AFOSR-82-1234.

5c. PROGRAM ELEMENT NUMBER.
Enter all program element numbers as they appear in the report, e.g. 61101A.

5d. PROJECT NUMBER.
Enter all project numbers as they appear in the report, e.g. 1F665702D1257; ILIR.

5e. TASK NUMBER. Enter all task numbers as they appear in the report, e.g. 05; RF0330201; T4112.

5f. WORK UNIT NUMBER.
Enter all work unit numbers as they appear in the report, e.g. 001; AFAPL30480105.

6. AUTHOR(S). Enter name(s) of person(s) responsible for writing the report, performing the research, or credited with the content of the report. The form of entry is the last name, first name, middle initial, and additional qualifiers separated by commas, e.g. Smith, Richard, J, Jr.

7. PERFORMING ORGANIZATION NAME(S) AND ADDRESS(ES). Self-explanatory.

8. PERFORMING ORGANIZATION REPORT NUMBER.
Enter all unique alphanumeric report numbers assigned by the performing organization, e.g. BRL-1234; AFWL-TR-85-4017-Vol-21-PT-2.

9. SPONSORING/MONITORING AGENCY NAME(S) AND ADDRESS(ES). Enter the name and address of the organization(s) financially responsible for and monitoring the work.

10. SPONSOR/MONITOR'S ACRONYM(S). Enter, if available, e.g. BRL, ARDEC, NADC.

11. SPONSOR/MONITOR'S REPORT NUMBER(S). Enter report number as assigned by the sponsoring/monitoring agency, if available, e.g. BRL-TR-829; -215.

12. DISTRIBUTION/AVAILABILITY STATEMENT. Use agency-mandated availability statements to indicate the public availability or distribution limitations of the report. If additional limitations/ restrictions or special markings are indicated, follow agency authorization procedures, e.g. RD/ FRD, PROPIN, ITAR, etc. Include copyright information.

13. SUPPLEMENTARY NOTES. Enter information not included elsewhere such as: prepared in cooperation with; translation of; report supersedes; old edition number, etc.

14. ABSTRACT. A brief (approximately 200 words) factual summary of the most significant information.

15. SUBJECT TERMS. Key words or phrases identifying major concepts in the report.

16. SECURITY CLASSIFICATION. Enter security classification in accordance with security classification regulations, e.g. U, C, S, etc. If this form contains classified information, stamp classification level on the top and bottom of this page.

17. LIMITATION OF ABSTRACT. This block must be completed to assign a distribution limitation to the abstract. Enter UU (Unclassified Unlimited) or SAR (Same as Report). An entry in this block is necessary if the abstract is to be limited.

PREVIOUS EDITION IS OBSOLETE.

STANDARD FORM 298 (REV. 5/2020)
Prescribed by ANSI Std. Z39.18

Distribution Statement

"Approved for Public Release; Distribution is Unlimited."

Final Research Report

ONR Award No. N00014-21-1-4007

NEMO Data Analysis and Environmental System Data Collection in Alternate Location Plan

Physical Oceanography Laboratory

Department of Marine and Environmental Sciences

Halmos College of Arts and Sciences

Nova Southeastern University

Period of Performance: 10/15/2020 – 01/14/2024 (at No Cost Extension)

Funding: $274,852.00

Technical Contact: Prof. Alexander V. Soloviev, Nova Southeastern University Halmos College of Arts and Sciences, 8000 N. Ocean Dr., Dania Beach, FL 33004; 954-262-3659; soloviev@nova.edu

Administrative contact: Cathy Harlan, Nova Southeastern University, 3301 College Ave., FL 33314; 954-262-5366; charlan@nova.edu

27 April 2024

Table of Content

1. INTRODUCTION

The Navy Electromagnetic Observatory (NEMO) in the Straits of Florida has been under development by the South Florida Ocean Measurement Facility (SFOMF). NEMO is designed to provide the observations required for development and verification of the new generation of models and algorithms for the noise reduction in naval magnetic surveillance systems.
The Physical Oceanography Laboratory at Nova Southeastern University's Halmos College of Arts and Sciences conducted observational, computational, and theoretical studies in oceanography and magnetohydrodynamics from 1998 through 2024 in support of the US Navy.

The long-term goal of this project is to support the development and validation of the magnetohydrodynamic (MHD) model of internal waves at the SFOMF range and planning the model assessment in alternate ocean conditions.

Our specific scientific objectives are as follows:

- Verify the MHD model with data from Navy Electromagnetic Observatory (NEMO) in the Straits of Florida.

- Identify suitable locations and plan deployment of the portable environmental data collection system, developed on a previous project, for the purpose of the MHD model validation in alternate environmental conditions.

2. ACCOMPLISHMENTS

2.1 Selection of Alternative Environment for Internal Wave Experiment

This part of the project is aimed at developing an alternative environment internal wave (IW) study compared to the Southeast Florida Shelf. The project covers only research, planning, and cost estimating tasks associated with the study. To conduct the experiments and analyze the data, future funding will be needed.

The objectives and requirements for the project to meet the US Navy's needs and future modeling efforts are as follows.

Objectives of the experiment

1. Test the portable system developed in contracts 1 and 2, upgrade as needed for new environment.

2. Conduct two 3-month experiments in a location that is known to have a regular IW field with a different ambient environment than that of South Florida, one that has been included in other studies. It is preferable to observe high-frequency IW and low background activity. Each 3-month experiment shall capture a large data set at different seasons under differing stratification profiles. This experiment will include:

• Different magnetic background field in new latitude and inclination

• Different oceanographic conditions

• Different IW field than what has been seen in SF

3. Determine ambient noise in a new environment.

4. Results to provide confidence in equipment and that the computational fluid dynamics and magnetohydrodynamics model NSU has been developing works in a different ambient environment.

Required equipment

• 6 low-resolution long range ADCPs

• 6 high-resolution short range ADCPs

• 3 magnetometers

• 6 pressure sensors

• 3 CTD chains

• Mooring equipment, acoustic releases, and tracking beacons

• Wave radar that reaches to location of array

• New equipment may be needed to make the moorings work in a new location (e.g., ADCP with directional surface wave package, Wirewalker, etc.) and to install the wave radar.

Option 1 – SE Alaska

A proposed location for deployment of the Portable Mooring Array is the Western Behm Canal in Alaska (Fig. 1.1). There is a Navy facility in the Western Behm Canal area–the Southeast Alaska Acoustic Measurement Facility (SEAFAC).

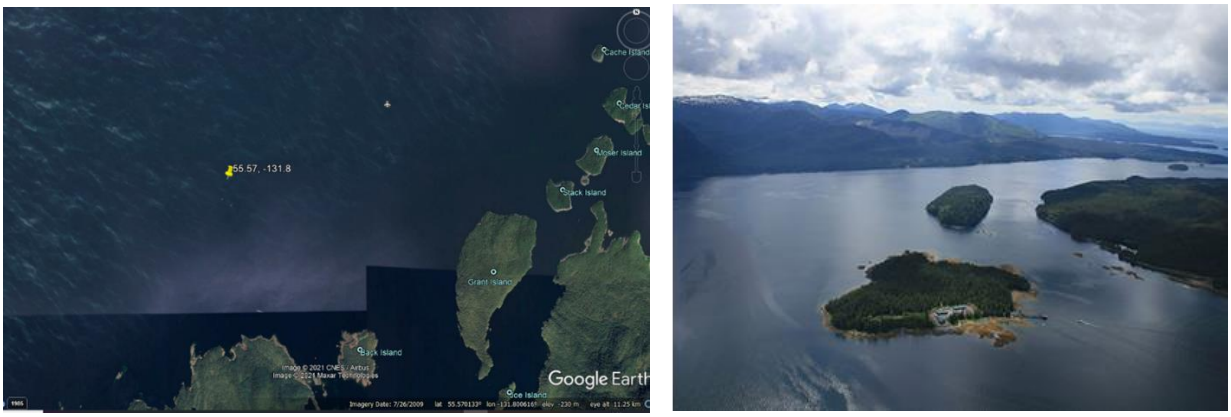

Figure 1.1. (left) Map of Southeast Alaska where the Behm Canal is located. Merrifield's et al. (2018) study site is shown by a yellow pin. (right) US Navy SEAFAC.

According to a previous study (Merrifield et al. 2018), this is a quiet, sheltered area much different than the coast of SE Florida inside the Florida Current. There is a known, regular IW field in the Western Behm Canal. Strong seasonality was observed in temperature in the upper 180 m, while salinity was consistently low in the near surface because of freshwater inputs to the fjord. Salinities below 150 m depth were close to offshore oceanic salinities (Merrifield et al. 2018). In the summer, the site has strong near-surface stratification and flow dominated by tides. This area was found to have stratified flows interacting within the fjords and to be a region of barotropic tidal energy conversion, IW generation, and vertical mixing (Merrifield et al. 2018). IW events are high frequency with periods of 5-15 minutes and 100-300 cycles per day, very close to N (buoyancy frequency) (Fig. 1.2).

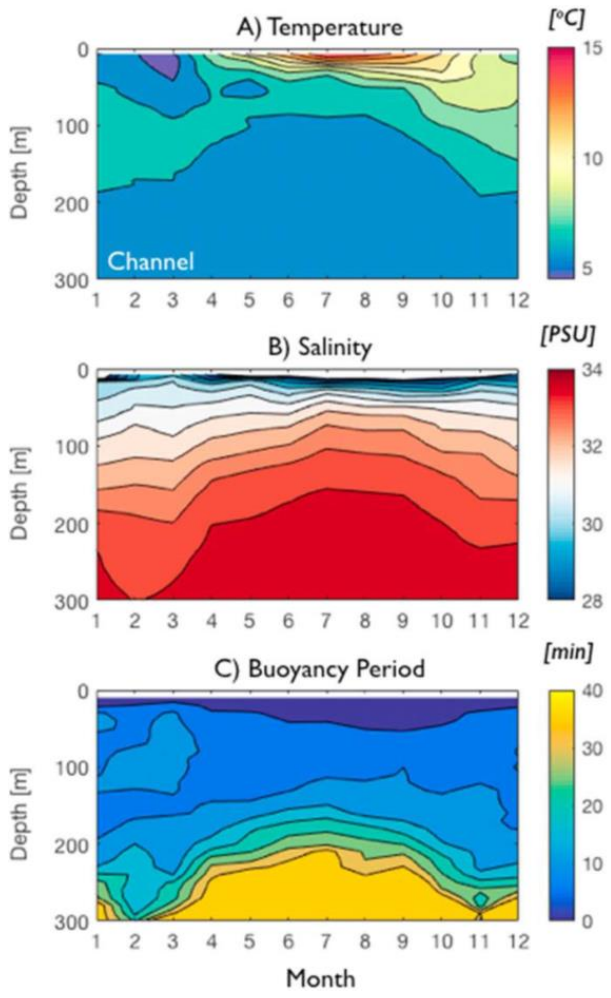

Figure 1.2. Seasonal (a) temperature contours every 1◦C and (b) salinity (contours every 1 psu) structure reconstructed from monthly averaged historical data between 2006 and 2017. (c) The buoyancy period shown by contours every 5 min representing that the high-frequency end of the IW spectrum was between 1 and 15 min in the upper 150 m with the highest values of stratification being observed at the near-surface in summer months. (After Merrifield's et al. 2018.)

The portable ADCP array, pressure sensors, and magnetometers can be installed at a depth of around 250 m, south of the Merrifield et al. (2018) study area, while the WaMoS HF radar (if installed at SEAFAC) can provide monitoring of surface waves and, possibly, surface current velocities in the area of research. The six ADCP and pressure moorings will provide information for the NSU computational fluid dynamics and magnetohydrodynamics model initialization, boundary conditions, and verification—which can be captured by a chain of CTD instruments installed on a surface mooring and, for example, by a Wirewalker carrying a high-resolution CTD and ADCP instruments.

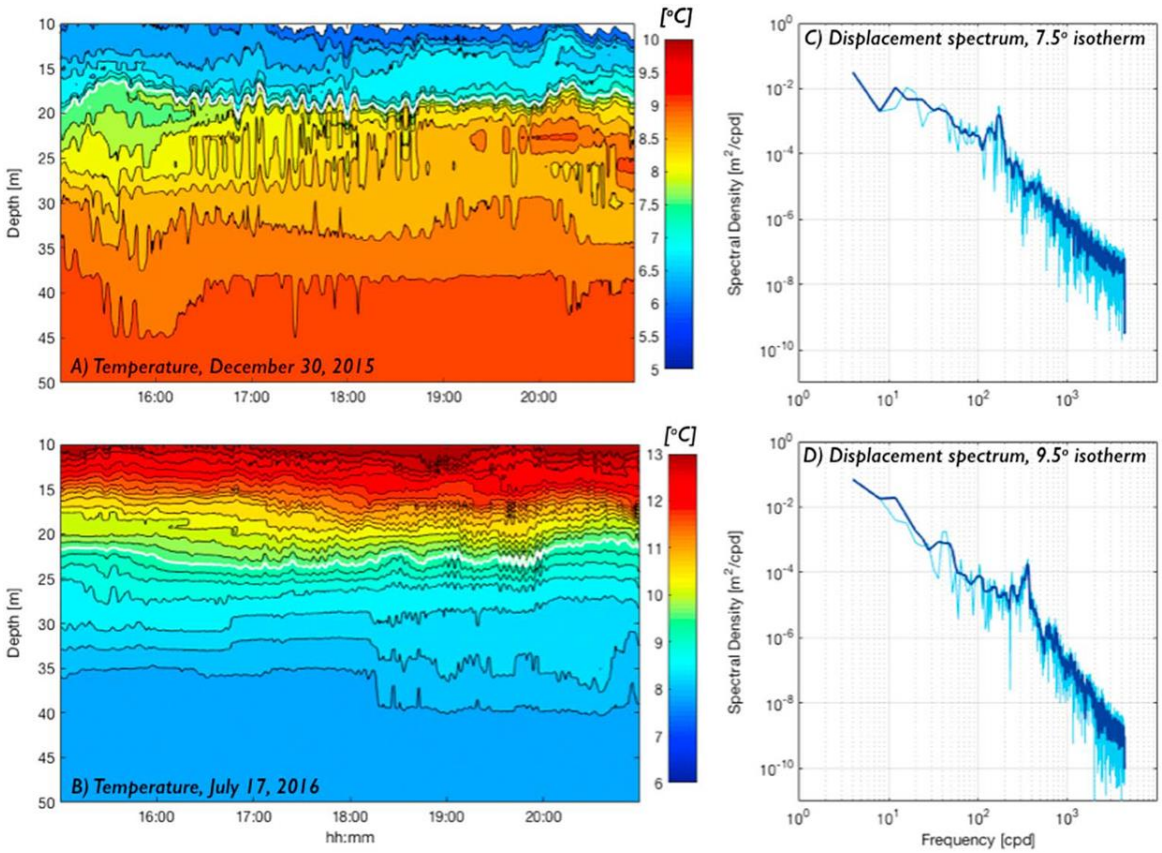

Figure 1.3. High-frequency internal waves activity observed in (a) December 2015 and (b) July 2016. Isotherms are shown every 0.25◦C. The displacement spectra are computed over 6 hours (c, d) for the 7.5◦C and 9.5◦C degree isotherms shown in white in (a, b) respectively. The dark blue line is a running average over seven adjacent bins. (After Merrifield's et al. 2018.)

Strong stratification in temperature and salinity develops in the upper 20 m of the fjord during summertime (see Fig. 1.3, lower left subplot). The winter stratification appears to be convectively unstable in temperature and neutral in salinity (see Fig. 1.3, upper left subplot). Buoyant convection may be the main source of high-frequency internal waves during wintertime. Note that the energy of wintertime high-frequency internal waves significantly exceeded summer values (Fig. 1.3, left column), while the frequency was lower during wintertime rather than summertime.

A preliminary estimate using the available information indicate that high-frequency internal waves with periods from 5 min to 15 min corresponds to wavelengths from 200 m to 800 m. Such relatively short internal waves compared to the depth of the fjord at the observational site will have a significantly reduced magnetic signature near the fjord bottom. The signature of high-frequency internal waves to be measured by bottom-based magnetometers may be too close

to the noise level of even very sensitive magnetometers, especially during summertime. This is the main challenge for conducting the IW magnetic signature experiment at the location in Alaska and an additional investigation is required. At the same time, the magnetic signature of tidal waves will practically have no decay with depth.

Option 2 – Southern California

Another alternative location is the California Bight from Palos Verdes Peninsula to the US Mexican border. Internal tides over abrupt topography in the Southern California Bight are known to create prominent IW solitons. Both high-frequency (5-30 min) and low-frequency (8-36 hr) internal waves have been observed (Beckenback and Terrill 2007 and others).

Most of IW soliton observations have been conducted at the San Diego locations. The San Diego area is, nevertheless, relatively shallow. The operational radius of the WaMoS radar is about 2 miles. The depth 2 miles offshore is still only about 50 m. The Portable mooring array cannot be very effective at such relatively small depths since the existing Teledyne Quartermaster ADCP instruments with a 150 kHz frequency will produce no more than 8 useful readings in the vertical direction.

Figure 1.4. California Palos Verdes.

A WaMoS radar can be installed at the lighthouse location (Fig. 1.4, right). This lighthouse is on the territory of the US Coast Guard. The ridge is expected to be within the operational radius of the WaMoS radar. There is a nearby commercial port.

At the Palos Verdes location, the ridge is expected to create regular, nonlinear tidally forced internal waves. Diurnal tidal forcing over the ridge and basin can lead to highly regular conversion of barotropic flow to baroclinic internal waves. The water depth is about 200 m at the ridge to 800 m westward (Fig. 1.4, left). The Portable array can be effectively used for the current velocity data collection within this depth range. The only problem is that we have not been able to find any information about the measurements of IW solitons at the Palos Verdes location, though, they are highly anticipated. Most of IW soliton observations have been performed either south (San Diego area) or north (Monterey Bay area) of Palos Verdes.

Next Steps

We have analyzed the proposed locations in Alaska and California including technical considerations, oceanographic patterns, environmental impacts, costs, and other factors. We have also searched for and found records of consistent high-frequency internal waves, which will allow us to avoid the situation of finding out after the experiment that we did not capture any useful IW soliton events. We have also implemented computational fluid dynamics and magnetohydrodynamics (ANSYS Fluent) to further evaluate the suitability of the alternative locations to meet the goal of this project.

2.2 Model Development for NEMO

The objective of this part of the project was to verify the magnetohydrodynamics (MHD) model with data from NEMO in the Straits of Florida and apply this model for an alternative environment. For this purpose, we have implemented high-resolution bathymetry in the combined computational fluid dynamics (CFD) and MHD model in the CFDM 2 model.
The concept is that as soon as we have an exact location of any observational site of interest for the US Navy, we will implement the high-resolution bathymetry in the CFD and MHD model. An algorithm for the implementation of the bottom topography has been developed in cooperation with the South Florida Ocean Measurement Facility (SFOMF) project Award N6426719C001.

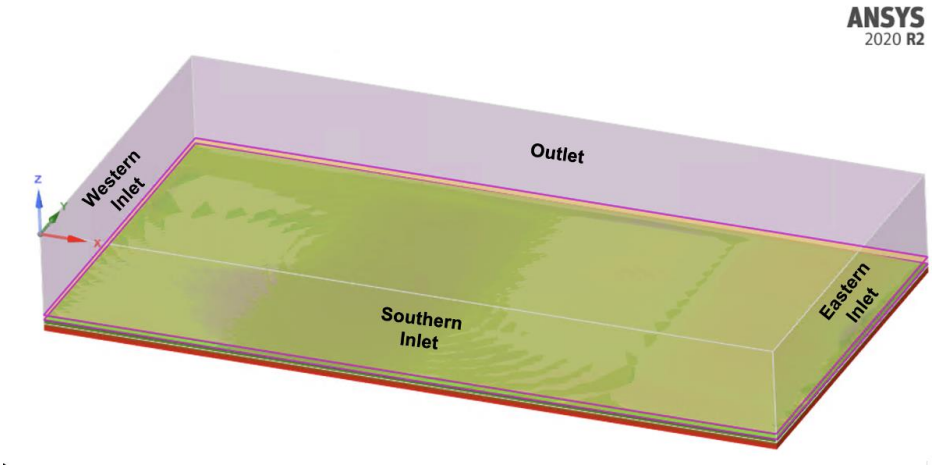

Figure 2.1. An example of high-resolution bathymetry for the CFD model in the Straits of Florida at a location similar to that of the NEMO (Vanderplow 2022). The domain is created in ANSYS SpaceClaim including bottom topography (green), and fluid zone (purple) split into the ADCP zone and the bottom layer. This is a location, which is similar to that of the NEMO (Miami Terrace); it does not have significant bottom elevation changes.

Prior to deploying the Nova Environmental Sensor Suite (NESS) at the NEMO site, we tested the possible influence of NEMO sensor infrastructure on the currents in the area of the deployment using our computational fluid dynamics model. The domain for this test can be seen in Figure 2.1. CFD model domain includes a box on the seafloor to represent the NEMO bottom sensor infrastructure (Fig. 2.2).

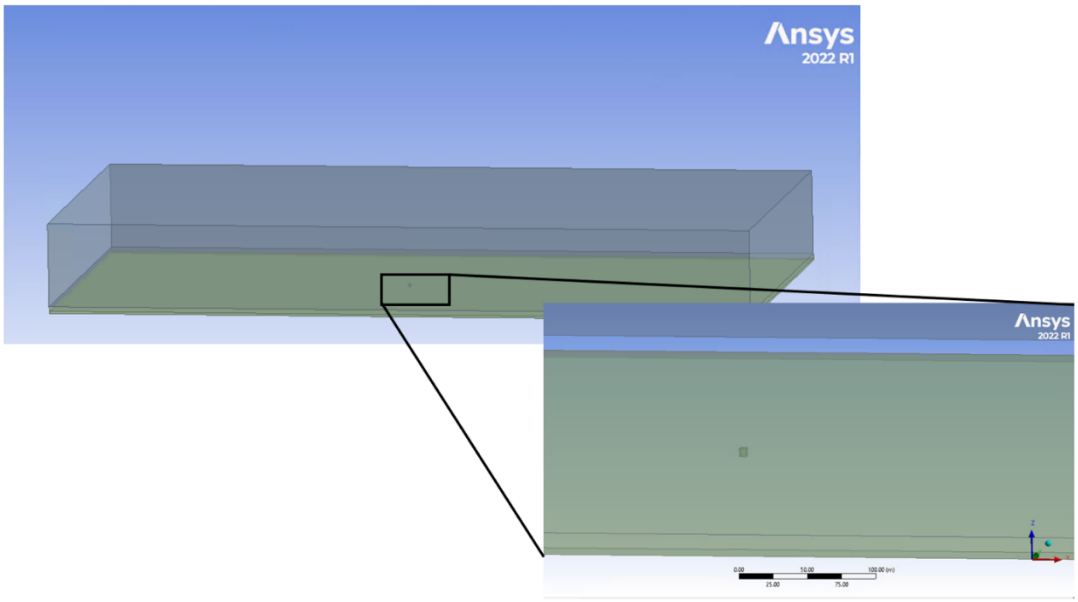

Figure 2.2. CFD model domain includes a box on the seafloor to represent the NEMO bottom sensor infrastructure.

This test is important since two magnetometers will be downstream from NEMO. Any current distortions caused by NEMO bottom infrastructure at the magnetometer location could lead to errors in magnetic signature data. This test has shown that the NEMO sensor infrastructure will have only a little or practically no impact on the current structure at the downstream magnetometer locations (Fig. 2.3).

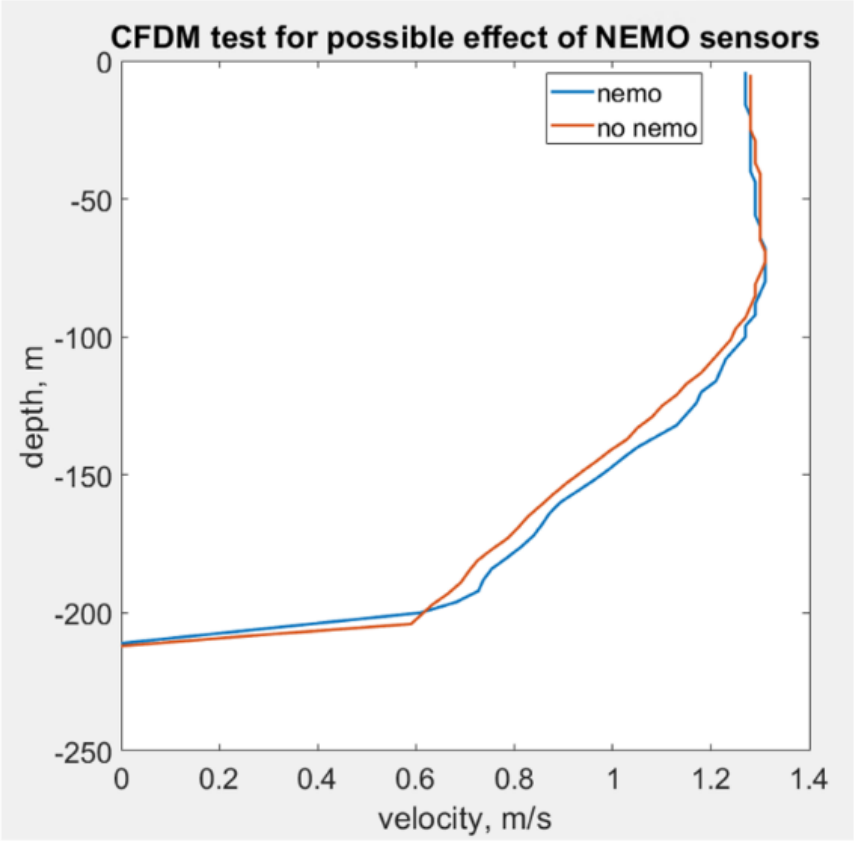

Figure 2.3. Comparison with (blue) and without (orange) NEMO sensor infrastructure box on the seafloor.

The CFD and MHD models were combined and upgraded into the CFDM 2 model. CFDM 2 was successfully tested in the US Navy contract N6426720C0045 and the related ONR Award N00014-22-1-2008. Figure 2.4 shows preliminary results of a comparison of CFDM 2 model results with in-situ data obtained from the NEMO bottom magnetometer.

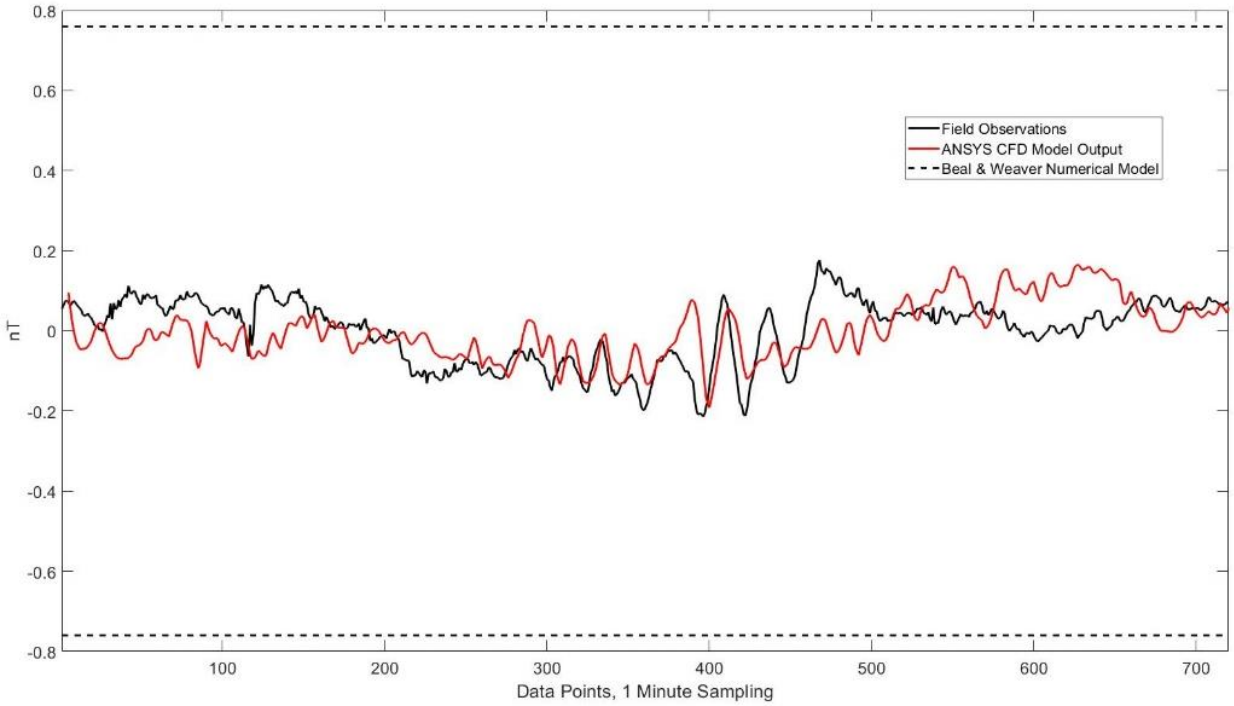

Figure 2.4. Preliminary comparison of CFDM 2 model results with in-situ data obtained with a NEMO bottom-mounted magnetometer in November 2022.

2.4 Data Analysis and Modeling for Alaska Alternative Location

This part of the project was aimed at developing an alternative environment internal wave (IW) study compared to the Southeast Florida Shelf. The project covered only research, planning, and cost estimation tasks associated with the study. To conduct the experiments and analyze the data, additional funds will be needed.

After discussions with our Navy partners, we focused on the alternative location in Alaska, near Back Island (Fig. 2.5). The main reason for this selection was that the vertical component of the Earth's magnetic field in Alaska was much larger than the horizontal one.

All observational data Alaska have been received from other investigators including the Merrifield et al. (2018) data, Navy ADCP data from SEAFAC and a Navy CTD cast.

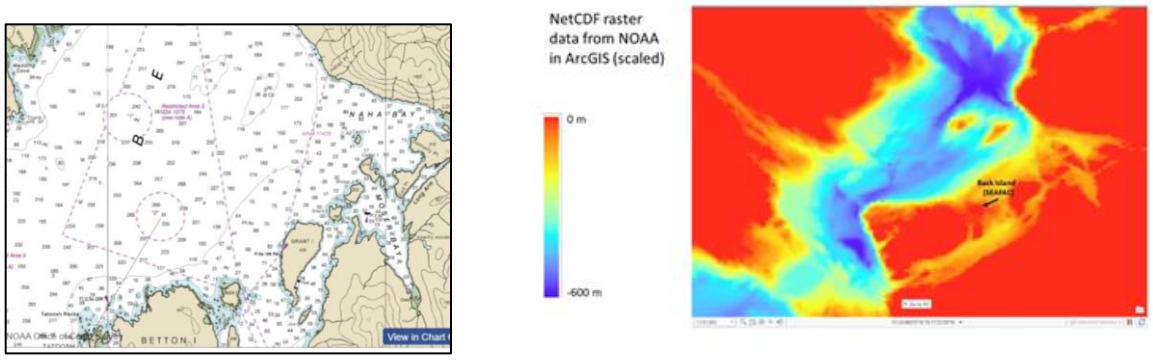

Figure 2.5. Bathymetry of the possible experimental location near Back Island (SEAFAC).

Preliminary analysis of the Alaska data (Merrifield, Otero, and Terrill, 2018) is shown in Figure 2.6 on the example of an internal wave soliton-type feature observed in the velocity field on January 10, 2016, at an approximately 98-meter depth (Fig. 2.7). We selected this example from the month of January because during summer months the soliton-type features at this location were observed mostly within the upper 50-meter layer of the ocean and are less likely to produce a measurable magnetic signature in the near-bottom layer.

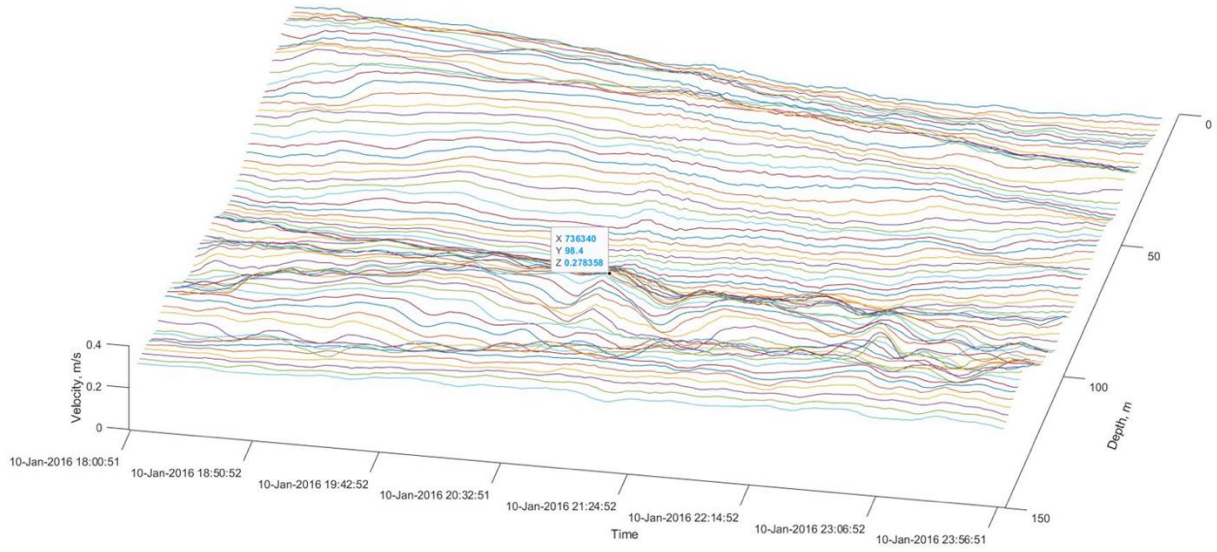

Figure 2.6. ADCP velocities on January 10, 2016. Note a soliton-type feature at a 98-meter depth.

A 264-meter wavelength estimate of the soliton-type feature under an assumption of two-layer stratification is shown in Figure 2.7.

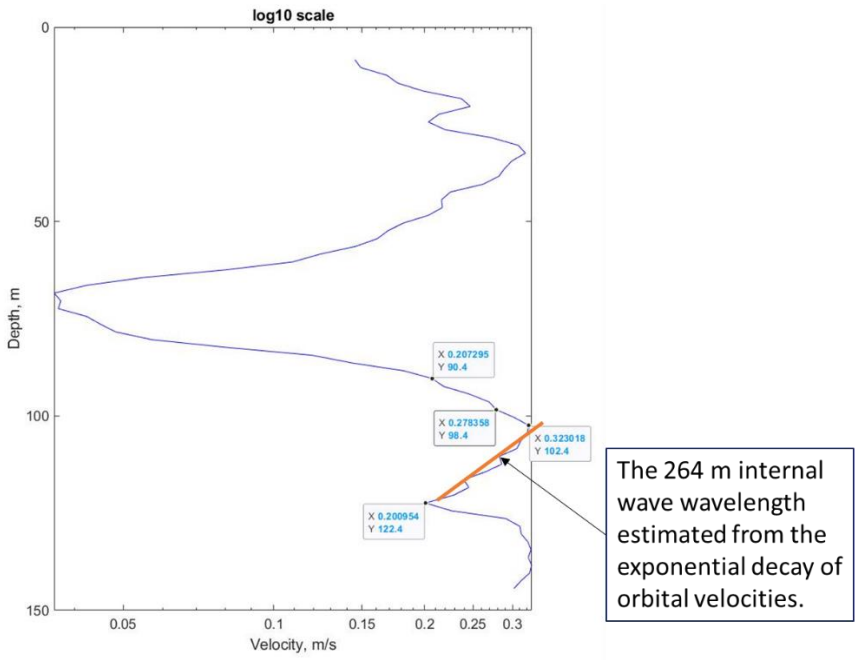

Figure 2.7. The estimate of the wavelength of the soliton-type feature (see Fig. 2.6) under an assumption of the exponential decay of internal wave orbital velocities.

This internal wave soliton feature was propagating within a layer of unstable temperature stratification (Fig. 2.8). Salinity might be compensating for the unstable temperature stratification, resulting in a stable density stratification, but salinity profiles were not available for this case. For comparison, Figure 2.9 shows temperature, salinity, and density profiles from a previous experiment.

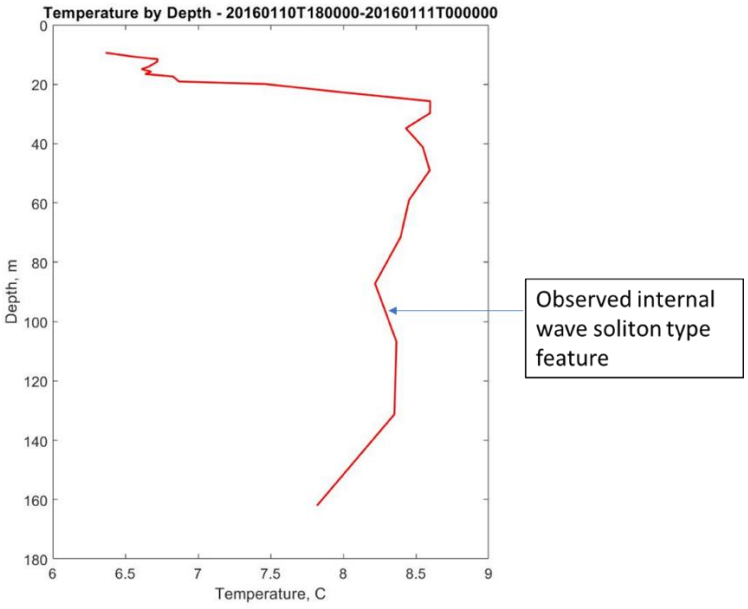

Figure 2.8. The vertical profile of temperature during the internal wave solution-type feature observation around a 98-meter depth in the layer of unstable temperature stratification. Salinity stratification was unknown. The depth in the Merrifield, Otero, and Terrill (2018) experiment analyzed here was 378 meters.

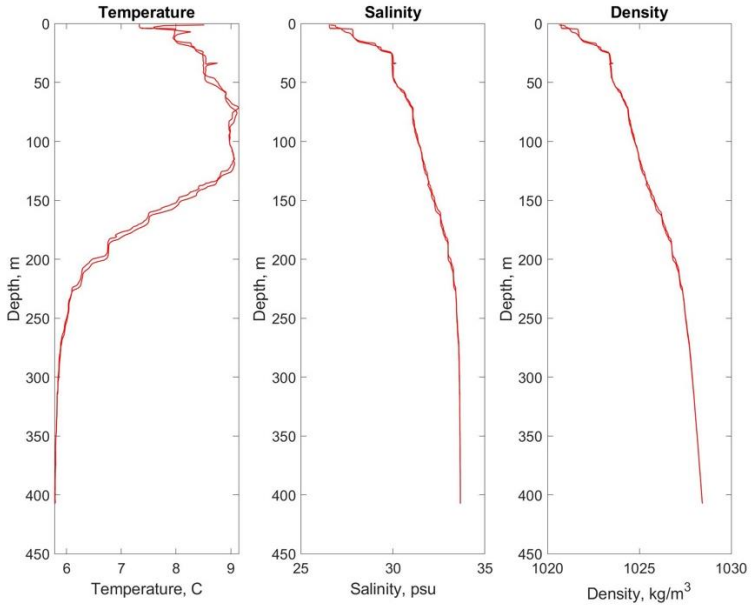

Figure 2.9. Vertical temperature, salinity, and density profile on November 28, 2021 at a somewhat different location near the Back Island (provided by the US Navy).

The estimate of the soliton-type feature wavelength shown in Figure 2.7 is a preliminary one because it is based on a two-layer stratification assumption and the information on the salinity and density component of stratification is not available. (During the measurements shown in Fig. 2.8, only vertical profiles of temperature were available.) Figure 2.9 shows the vertical profile of temperature salinity, and density taken on 28 November 2021 though at somewhat different location near Back Island.

The origin of the soliton-type feature in Figure 2.6 is not completely clear as well since it might develop in a convectively unstable layer. For the consideration of Alaska as an alternative experimental location, it is most important to find that these soliton-type features produce a measurable magnetic signature in the near-bottom layer.

A preliminary estimate for the magnetic signature of the phenomenon resembling an internal wave solution with a wavelength of about 260 m (Figs. 2.6) observed at an approximately 100 m depth was produced with the NSU CFDM 2 model (Figs. 2.10, 2.11). The model provides a rough estimate of the magnetic signature of an internal wave in the Alaska location based on the

data provided by the Navy and the local magnetic field (North 1.53669×10^{-5} T, East 5.0157×10^{-6} T, Vertical 5.2589×10^{-5} T).

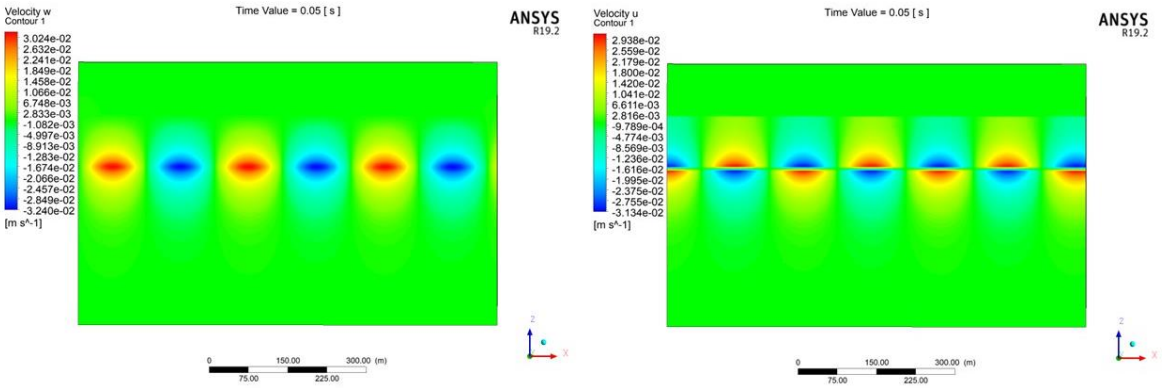

Figure 2.10. Vertical velocity (left) and x velocity (right) of the modeled internal wave with a 260 m wavelength and 1 m amplitude at 1 depth of 100 m.

Relatively short internal waves compared to the depth of the fjord at the observational site will have a significantly reduced magnetic signature near the fjord bottom. The magnetic signature estimate in Figure 2.11 has been calculated for the internal wave of a 10 m amplitude. As expected, the vertical component of the magnetic signature in Alaska dominates over the horizontal ones because the angle of the magnetic induction lines is almost vertical. This is different from Florida's magnetic field.

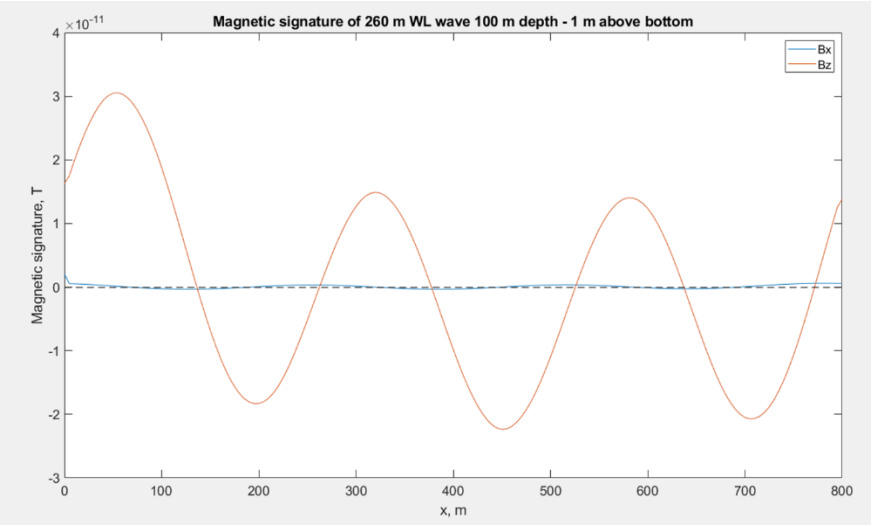

Figure 2.11. X and Y components of the magnetic signature of the CFDM 2 model of internal wave in the Alaska alternate location. The dashed line shows the magnetic sensitivity of the best magnetometers ($50X10^{-15}$ T).

2.4 Conclusions

The results of our investigation suggest that the signature of high-frequency internal waves to be measured by bottom-based magnetometers may be too close to the noise level of even very sensitive magnetometers. This is the main challenge for conducting the IW magnetic signature experiment at the location in Alaska.

After consulting with our Navy partners, the final location for an alternative environment internal wave experiment was selected in Scotland.

3. SELECTED REFERENCES

Beckenbach, E., and E. Terrill, 2008. Internal tides over abrupt topography in the Southern California Bight: Observations of diurnal waves poleward of the critical latitude. *Journal of Geophysical Research* 113, C02001.

Inall, M., T. Rippeth, C. Griffiths, and P. Wiles, 2005. Evolution and distribution of TKE production and dissipation within stratified flow over topography. *Geophysical Research Letters* 32, L08607.

Merrifield, S., Otero, M., & Terrill, E., 2018. Observations of shelf exchange and high-frequency variability in an Alaskan fjord. *Journal of Geophysical Research* 123, 4720–4734.

Vanderplow, B., Kluge, J.A., Soloviev, A.V., Dodge, R., Wood, J., Evans, J., Venezia, W., & Ferrar, M. 2022 Measurement and modeling of small-scale to meso-scale features in a western boundary current. Submitted to *Geophysical Research Letters.*

4. TRAINING AND PRODESSIONAL DEVELOPMENT

- MS and PhD student attendance and presentation at major conferences.
- ANSYS Computational Fluid Dynamics tutorials taken by students.
- CUI security tutorial taken as required.

5. RESULTS DISSEMENATION

Kluge, J., Vamderplow, B., Dean, C., Evans, J., Soloviev, A. (2024). Comparison of Glider and Mooring Data in a Strong Western Boundary Current. Submitted to *Journal of Atmospheric and Oceanic Technology*. in review

Vanderplow, B., Kluge, J.A., Soloviev, A.V., Dodge, R., Wood, J., Evans, J., Venezia, W., & Farrar, M. (2022). Measurement and modeling of small-scale to meso-scale features in a western boundary current. *Ocean Modeling.* In revision.

6. HONORS AND AWARDS

- Dr. Alexander Soloviev, Nova Southeastern University Provost's Research and Scholarship Award, 2021.
- Breanna Vanderplow, Outstanding Oral Presentation Award. American Meteorological Society's 35th Conference on Hurricanes and Tropical Meteorology. New Orleans, 2022.

7. DISTRIBUTION STATEMENT

"Approved for Public Release; Distribution is Unlimited."

8. PARTICIPANTS (because of the COVID-19 quarantine the project was for approximately 2 years at no cost extension, months worked varied)

First Name: Alexander Last Name: Soloviev
Project Role: PD/PI
National Academy Member: N

First Name: Breanna Last Name: Vanderplow
Project Role: Laboratory Supervisor / Graduate Student
National Academy Member: N

First Name: John Last Name: Kluge
Project Role: Graduate Research Associate / Graduate Student
National Academy Member: N

First Name: Alfredo Last Name: Quezada
Project Role: Graduate Research Assistant / Graduate Student
National Academy Member: N

First Name: Megan Last Name: Miller
Project Role: Graduate Research Assistant / Graduate Student
National Academy Member: N

First Name: Stephanie Last Name: Ball
Project Role: Graduate Research Assistant / Graduate Student
National Academy Member: N

First Name: Geoffrey Last Name: Morrison
Project Role: Senior Ocean Engineer
National Academy Member: N

First Name: Terry Last Name: Thompson
Project Role: Senior Ocean Engineer
National Academy Member: N

First Name: Luba Last Name: Solonenko
Project Role: Project Coordinator
National Academy Member: N

First Name: Brian Last Name: Ettinger
Project Role: Boat Captain / Field Operations
National Academy Member: N

First Name: Mikayla Last Name: Craven
Project Role: Graduate Research Assistant / Graduate Student
National Academy Member: N

First Name: Georgia Last Name: Parks
Project Role: Graduate Research Assistant / Graduate Student
National Academy Member: N

First Name: Ian Last Name: Lundy
Project Role: Intern
National Academy Member: N
Graduated and left the project.

Countries of Collaboration: N/A

Countries of Collaboration on other lab projects: Germany, Canada, South Korea.

9. PRODUCTS

a. MS Thesis

Quezada, A. (2023). Investigating Patterns of Current Velocities, Nutrient Transport, and the Diel Vertical Migration in the Southeastern Florida Shelf Using Robotic Instruments. Department of Marine and Environmental Sciences, Halmos College of Arts and Sciences, Nova Southeastern University. MS Degree Thesis. Defended on December 7, 2023.

Miller, M. (2023). Computational Fluid Dynamics Modeling of Internal Wave Interactions on Conch Reef, Florida Keys. Department of Marine and Environmental Sciences, Halmos College of Arts and Sciences, Nova Southeastern University. MS Degree Thesis. Defended on December 8, 2023.

b. PhD Dissertation

Kluge, J. A. (2023). Characterizing Ocean Surface and Internal Wave Magnetic Signatures: Laboratory, Field, and Glider-based Observations. Department of Marine and Environmental Sciences, Halmos College of Arts and Sciences, Nova Southeastern University. PhD Dissertation. Defended on November 30, 2023.

Vanderplow, B. (2023). Microscale to Mesoscale Modeling of the Ocean Under Tropical Cyclones: Effects of Sea Spray and Surfactants on Tropical Cyclone Intensity and Air-Sea Gas Exchange. Department of Marine and Environmental Sciences, Halmos College of Arts and Sciences, Nova Southeastern University. PhD Dissertation. Defended on November 30, 2023.

REPORT DOCUMENTATION PAGE

1. REPORT DATE	2. REPORT TYPE	3. DATES COVERED	
		START DATE	END DATE
20240427	Final	Oct. 15, 2020	Jan. 14, 2024

4. TITLE AND SUBTITLE

NEMO Data Analysis and Environmental System Data Collection in Alternate Location Plan

5a. CONTRACT NUMBER	5b. GRANT NUMBER	5c. PROGRAM ELEMENT NUMBER
	N00014-21-1-4007	
5d. PROJECT NUMBER	**5e. TASK NUMBER**	**5f. WORK UNIT NUMBER**

6. AUTHOR(S)

Soloviev, Alexander. V.

7. PERFORMING ORGANIZATION NAME(S) AND ADDRESS(ES)
Nova Southeastern University
3301 College Ave, Fort Lauderdale, FL 33314

8. PERFORMING ORGANIZATION REPORT NUMBER

9. SPONSORING/MONITORING AGENCY NAME(S) AND ADDRESS(ES)	10. SPONSOR/MONITOR'S ACRONYM(S)	11. SPONSOR/MONITOR'S REPORT NUMBER(S)
Office of Naval Research	ONR	

12. DISTRIBUTION/AVAILABILITY STATEMENT
Approved for public release; distribution unlimited.

13. SUPPLEMENTARY NOTES

14. ABSTRACT

. The goal of this project is to support the development and validation of the electromagnetic (EM) model of internal waves (IWs) at Navy Electromagnetic Observatory (NEMO) in the Straits of Florida and planning the model assessment in alternate ocean environmental conditions.

Respectively, our specific scientific objectives are as follows:

- Verify the EM model with data from NEMO
- Identify suitable locations and plan deployment of the portable environmental data collection system, developed on a previous project, for the purpose of electromagnetic model validation in alternate environmental conditions.

In this project, the Navy and NSU have worked together to identify suitable alternate locations to deploy the portable environmental data collection system. The results of this investigation suggested that at the Alaska location the signature of high-frequency IWs to be measured by bottom-based magnetometers may be too close to the noise level of even very sensitive magnetometers. This is the main challenge for conducting the IW magnetic signature experiment at the location in Alaska. Assessments of potential sites have been discussed with the Navy. After consulting with our Navy partners, the final location for an alternative environment internal wave experiment was selected in Scotland, UK

The anticipated outcome of the research is an advanced MHD model verified in the western boundary current (Florida Current) and at an alternate location with different environmental conditions. Potential applications of the results of this study for DoD include locating underwater vehicles from aircraft. Other applications involve geophysical prospecting for oil and minerals under the seafloor and for

archeological investigations, and environmental assessment studies.

15. SUBJECT TERMS

Straits of Florida, Southern California, Alaska, Scotland, ocean circulation, internal waves, CFD, MHD, numerical modeling, air-sea interaction

16. SECURITY CLASSIFICATION OF:			17. LIMITATION OF ABSTRACT	18. NUMBER OF PAGES
a. REPORT	b. ABSTRACT	C. THIS PAGE		
U	U	U	UU	

REPORT DOCUMENTATION PAGE

1. REPORT DATE	2. REPORT TYPE	3. DATES COVERED	
		START DATE	END DATE
20240427	Final	Oct. 15, 2020	Jan. 14, 2024

4. TITLE AND SUBTITLE

NEMO Data Analysis and Environmental System Data Collection in Alternate Location Plan

5a. CONTRACT NUMBER	5b. GRANT NUMBER	5c. PROGRAM ELEMENT NUMBER
	N00014-21-1-4007	
5d. PROJECT NUMBER	**5e. TASK NUMBER**	**5f. WORK UNIT NUMBER**

6. AUTHOR(S)

Soloviev, Alexander. V.

7. PERFORMING ORGANIZATION NAME(S) AND ADDRESS(ES)	8. PERFORMING ORGANIZATION REPORT NUMBER
Nova Southeastern University 3301 College Ave, Fort Lauderdale, FL 33314	

9. SPONSORING/MONITORING AGENCY NAME(S) AND ADDRESS(ES)	10. SPONSOR/MONITOR'S ACRONYM(S)	11. SPONSOR/MONITOR'S REPORT NUMBER(S)
Office of Naval Research	ONR	

12. DISTRIBUTION/AVAILABILITY STATEMENT

Approved for public release; distribution unlimited.

13. SUPPLEMENTARY NOTES

14. ABSTRACT

. The goal of this project is to support the development and validation of the electromagnetic (EM) model of internal waves (IWs) at Navy Electromagnetic Observatory (NEMO) in the Straits of Florida and planning the model assessment in alternate ocean environmental conditions.

Respectively, our specific scientific objectives are as follows:

- Verify the EM model with data from NEMO
- Identify suitable locations and plan deployment of the portable environmental data collection system, developed on a previous project, for the purpose of electromagnetic model validation in alternate environmental conditions.

In this project, the Navy and NSU have worked together to identify suitable alternate locations to deploy the portable environmental data collection system. The results of this investigation suggested that at the Alaska location the signature of high-frequency IWs to be measured by bottom-based magnetometers may be too close to the noise level of even very sensitive magnetometers. This is the main challenge for conducting the IW magnetic signature experiment at the location in Alaska. Assessments of potential sites have been discussed with the Navy. After consulting with our Navy partners, the final location for an alternative environment internal wave experiment was selected in Scotland, UK

The anticipated outcome of the research is an advanced MHD model verified in the western boundary current (Florida Current) and at an alternate location with different environmental conditions. Potential applications of the results of this study for DoD include locating underwater vehicles from aircraft. Other applications involve geophysical prospecting for oil and minerals under the seafloor and for archeological investigations, and environmental assessment studies.

15. SUBJECT TERMS				
Straits of Florida, Southern California, Alaska, Scotland, ocean circulation, internal waves, CFD, MHD, numerical modeling, air-sea interaction				
16. SECURITY CLASSIFICATION OF:			**17. LIMITATION OF ABSTRACT**	**18. NUMBER OF PAGES**
a. REPORT	**b. ABSTRACT**	**C. THIS PAGE**		
U	U	U	UU	

SF298

January 27, 2024

ONR Award No. N00014-21-1-4007

NEMO Data Analysis and Environmental System Data Collection in Alternate Location Plan

PI: Dr. Alexander V. Soloviev

1. Problems, delays, or adverse conditions will materially impair your ability to meet the objectives of this award. This disclosure must include a statement of the action taken, or contemplated, and any assistance needed to resolve the situation.

During the project the COVID-19 pandemic created delays in the data analysis, computer modeling, and dissemination of scientific results. These factors delayed the data analysis and publications for this project. The result was extending the project (no cost extension) until January 14, 2024.

2. Favorable developments which will enable you to meet schedules and objectives sooner or at less cost than anticipated or produce more or different beneficial results than originally planned.

Favorable development during the project was our strong partnership with the US Navy (Carderock Division and South Florida Ocean Measurement Facility). Additionally, our previous experience in using computational fluid dynamics modeling helped us to evaluate Alaska as an alternative environment for a high-latitude internal wave experiment.

Measurement and modeling of small-scale to meso-scale features in a western boundary current

Vanderplow, Breanna[1], Kluge, John A.[1], Soloviev, Alexander V.[1], Dodge, Richard[1], Wood, Jon[2], Evans, Johanna[3], Venezia, William[3], and Farrar, Michael[3]

[1]Nova Southeastern University, Dania Beach, FL, USA
[2]Ocean Data Technologies, Inc., Hyannis, MA, USA
[3]Naval Surface Warfare Division Carderock Division, Fort Lauderdale, FL, USA

Key points:

- We propose a modeling approach for predicting the ocean circulation in strong currents in the range from small-scales to sub-mesoscales.
- This approach has been verified with field data from the Straits of Florida.
- We anticipate this result is a starting point for sophisticated high-resolution models applicable to western boundary currents.

Key words: western boundary current, ocean currents, three-dimensional modeling, small-scale, sub-mesoscale, mooring array, model verification

Index: 4512, 4524, 4534, 4562, 4576, 4263

Abstract

Coastal ocean circulation models typically have horizontal resolution starting from 1 km. Predicting ocean circulation on sub-mesoscales is still a challenge. Here we propose a new approach to address this challenge. A high resolution, three-dimensional computational fluid dynamics (CFD) model domain containing inlets and an outlet has been developed and verified with field data from the Straits of Florida. For the model verification, a 6 ADCP mooring array in a rectangular shape was deployed 8 miles offshore on the Miami Terrace. The data from 5 ADCP moorings were used to produce the inlet boundary conditions updated every 1 minute. The sixth ADCP in the center of the outlet was used for the model verification. This approach has demonstrated good predictive ability in the challenging environment of a strong western boundary current. We anticipate our work to be a starting point for sophisticated prediction models applicable to western boundary currents in the range from small-scales to sub-mesoscales.

Plain Language Summary

Predicting ocean circulation remains challenging because of modelling capabilities such as resolution. To address this issue we have developed a high resolution three-dimensional model for strong ocean currents such as the Gulf Stream. The model has been verified with field data from the Straits of Florida. Field data was collected during an experiment 8 miles offshore of Southeast Florida using equipment to measure ocean current velocities. The model has demonstrated the ability to predict ocean circulation at a high resolution in a challenging environment with strong, variable currents. We anticipate this model to be applicable to other locations such as the Kuroshio Current or Agulhas Current where circulation on small to medium scales is difficult to predict.

1. Introduction

1.1 Challenges of modeling submesoscale features in western boundary currents

Sub-mesoscale flows have a length of 0.1-10 km and are sometimes difficult to observe in the ocean and model because of their short timescales and small lengthscales (Thomas, Tandon & Mahadevan, 2008; Bachman et al., 2017; Su et al., 2018). Some ocean features such as ocean fronts and internal wave solitons require even smaller spatial resolution starting from a few meter scales. Resolving the range of from small-scales **(below 0.1 km)** to sub-mesoscales is a big challenge in a strong current like a western boundary current. We are developing an approach to address this challenge using field and computational experimentation in the Straits

of Florida as an example. **This method uses a large scale map approach to look at a region of Straits of Florida with a high level of detail to resolve small to meso-scale oceanic features.**

The Florida Current, with current speeds up to ~2.5 m/s, is a part of the North Atlantic Western Boundary Current. According to Stommel (1965), the Loop Current in the Gulf of Mexico becomes the Florida Current in the Straits of Florida and the Gulf Stream leaving the Straits of Florida. The Florida Current is characterized by intense mesoscale **(>10 km)**, sub-mesoscale, and small-scale variability including a variety of features such as meanders, eddies, fronts, and internal waves that are caused by the flow over a highly variable bottom topography and air-sea interaction. There is also a seasonally modulated undercurrent/countercurrent jet attached to the continental shelf of Florida (Soloviev et al., 2017).

Current circulation on the Southeast Florida shelf is associated with the many processes occurring in the Florida Current range in time and space scales, including inhomogeneities caused by bottom topography, barotropic and baroclinic tides, meteorological forcing, and stratified current structure. Variations in the Florida Current caused by seasonal and interannual variability represent ~70% of the total variance attributed to less than annual periods (Schott et al., 1988; Meinen et al., 2010). In addition, frontal mesoscale and sub-mesoscale eddies periodically develop in the Straits of Florida. The Florida Current also has prominent current oscillations on ~10-hour time scales observed on the Florida shelf. These oscillations are seasonally modulated and reach a maximum during the summer (Soloviev, Luther, and Weisberg, 2003; Soloviev et al., 2003).

The Florida Current reveals seasonal to tidal variability but is generally steady over a timescale of years. Transport is highest in the spring and summer and decreases in the fall, associated with along-channel winds in the Straits of Florida (Lee and Williams, 1988) and wind forcing in the North Atlantic (Schott et al., 1988). Wind forcing and continental shelf waves lead to meanders and frontal eddies in the Florida current, resulting in variability at timescales of days to weeks (Davis et al., 2008). Large cyclonic, cold-core eddies that form near the Dry Tortugas move northeast on the western side of the Florida Current (Lee et al., 1995) and eventually elongate into mesoscale and sub-mesoscale eddies near the middle and upper Florida Keys (Haus et al., 2000). Sub-mesoscale frontal eddies are also generated near offshore meanders in the Florida Current, which lead to water mass exchange between the Florida Current and the shelf

(Haus et al., 2004). Internal waves are generated from fronts or eddies in the Florida Current and tidal forces (Davis et al., 2008). Internal tidal velocity fluctuations of up to 0.5 m/s have been observed in the surface waters of the Straits of Florida (Pillsbury, 1891; Parr, 1937; Schimtz and Richardson, 1968). Soloviev, Luther, and Weisberg (2003) observed similar oscillations with periods of 10 hours and a seasonal modulation that peaks during the summer. The 10-hour period aligns closely with the semidiurnal tidal constituents present in the Florida Straits (M_2 12.42 hours and S_2 12 hours) (Soloviev, Luther, and Weisberg, 2003). However, no definitive explanation for the 10-hour internal wave oscillation has been established since the time of the Pillsbury (1891) discovery.

1.2 A new approach to modeling in the range of small-scale to sub-mesoscale features in a western boundary current - computational fluid dynamics model

Replicating ocean dynamics on sub-mesoscales is challenging in numerical models. Here we have implemented an engineering type modeling - Computational Fluid Dynamics (CFD). ANSYS Fluent CFD software provides a large assortment of physical model capabilities, including flow, turbulence, multiphase, and heat transfer that have been validated and produce highly accurate results. CFD, while computationally expensive, provides a rigorous nonlinear treatment of the Navier-Stokes equations involved in modeling mass and momentum transfer, critical to fluid dynamics. By discretizing CFD domains in space and time, the system of equations is formed and implemented into a domain mesh and timesteps during the simulation (Windt, Davidson and Ringwood, 2018). CFD-based modeling of ocean processes can capture small-scale to mesoscale features and provide high-resolution results to better understand flow and currents in places challenging to study, such as western boundary currents like the Florida Current.

Soloviev, Fujimura, and Matt (2012), Soloviev et al. (2014 and 2017), and Vanderplow et al. (2020) applied CFD for air-sea interaction studies. CFD has also been used to study various fluid dynamics and related oceanographic processes. Stern et al. (2014) applied CFD to naval architecture and ocean engineering, Wang et al. (2012) studied small-scale wave breaking using CFD simulation, and Koo et al. (2014) and Yoon et al. (2013) modeled wave run-up and turbulent flow around vertical cylinders. Simonetti et al. (2015) compared two CFD turbulence models, k-w SST and LES, for application to oscillating water column wave energy converters

and found that while both methods provided agreeable results to their measurements, the LES model results were closer to experimental data, although it was more computationally expensive. Sjökvist et al. (2017) utilized CFD to simulate wave energy converters and verify their models using experimental results. CFD has aided in studying the interaction between oil and dispersants, which is critical to oil spill mitigation (Soloviev et al., 2016). Soloviev, Dean, & Fujimura (2015) used CFD to study salinity fluxes in freshwater lenses and their connection to the ocean barrier layer (Lukas and Lindstrom, 1991).

In this work we demonstrate that validated CFD simulations combined with field data provide an effective way to assimilate available oceanic information and predict small-scale to sub-mesoscale processes in the area of interest within a certain time range.

2. Measurements

The deployment in the Straits of Florida was designed to measure ocean currents, water conductivity-temperature-depth, and bottom pressure variability necessary to develop a CFD model of the Florida Current in the study area. The mooring array deployed 8 miles offshore at roughly 250 m depth contained fourteen moorings: six acoustic Doppler current profiler (ADCP) moorings intended to measure ocean current velocity profiles, five pressure moorings intended to measure bottom pressure (not used in this paper), three temperature-conductivity-depth (CTD) mooring strings to measure water density throughout the water column. The moorings were deployed in a rectangular pattern (Fig. 1a) across the shelf. ADCP moorings were spaced ~850 m apart from one another, as were the CTD mooring chains.

Current measurements were obtained with upward-looking Teledyne RD Instruments 150 kHz Quartermaster ADCPs placed 8 m from the seafloor and looked upwards with a 4 m vertical resolution (ensemble-averaged every 1 minute). Each ADCP was fixed with a Deepwater Buoyancy, Inc. 49” syntactic spherical buoy and protected by a stainless-steel mounting cage. A 900 kg railroad wheel anchor with a 3/8” proof coil chain was used as an anchor for each mooring. A Teledyne Benthos model R2k acoustic release was placed halfway between the anchor and buoy. For the pressure moorings, an RBR, Ltd RBRquartz^3 Q digiquartz high-accuracy pressure transducer was mounted using clamps in a stable bottom-mounted stainless-steel frame and cast concrete anchor ~20 cm above the seafloor. Trawl floats were used to add 25

kg of net positive buoyancy. The pressure moorings were also equipped with a Xeos satellite beacon and Teledyne Benthos R500 acoustic release. The CTD mooring strings consisted of eight Sea-Bird Electronics, Inc. SBE-37SMP CTD sensors spaced 25 m apart along the mooring line, beginning at 22 m below the sea surface to ~197 m below the sea surface. A Stable-Moor torpedo-shaped syntactic foam buoy was used for stability (620 kg of positive buoyancy) at the top of the mooring wire (Fig. 1b). This type of buoy effectively improved the lift-to-drag ratio of the CTD mooring and, therefore, increased overall mooring performance and data quality. The CTD moorings also contained a spherical backup buoy, A Teledyne Benthos model R12k acoustic release, and a 1550 kg railroad wheel anchor. Figure 1c shows a contour plot of the northward velocity component from an ADCP deployed during January-March 2020.

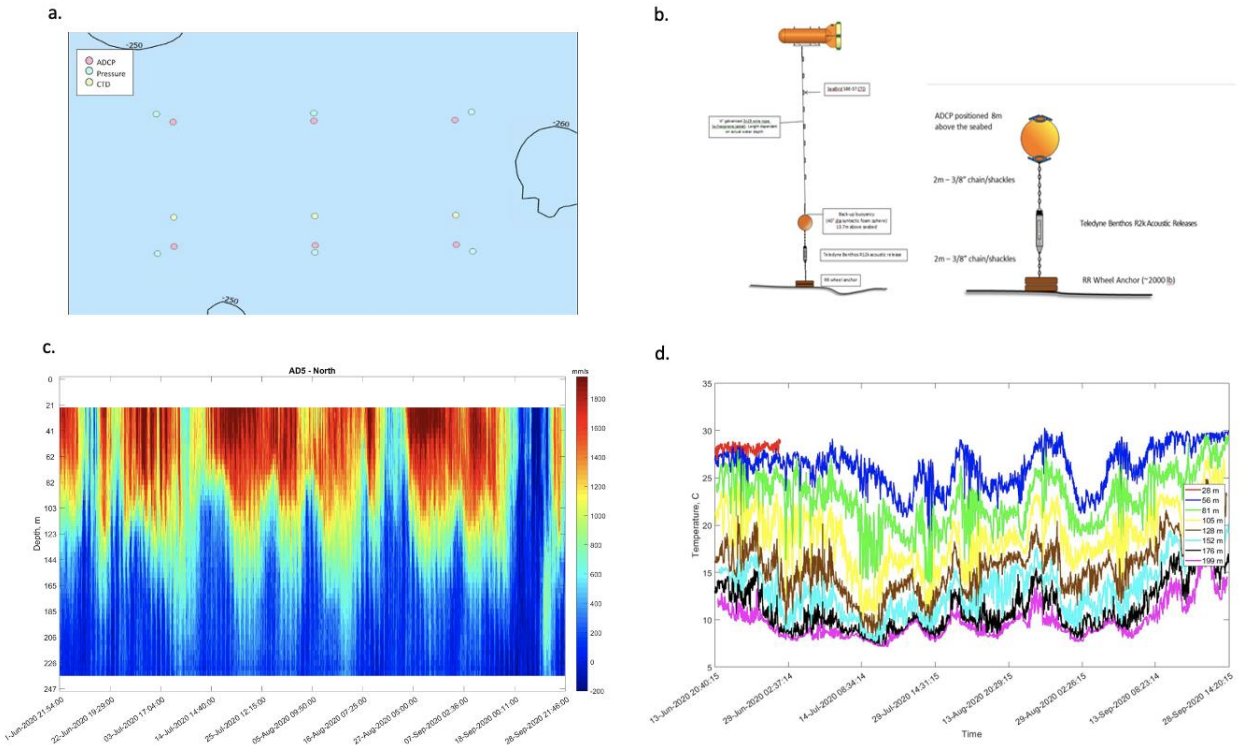

Figure 1. (a.) Mooring array design in the Straits of Florida showing location of the moorings and the bottom topography in the area of interest. (b.) Mooring design for CTD chains and ADCP moorings. (c.) Northward velocity component from an ADCP. (d.) Temperature time series from a CTD mooring.

3. Sub-mesoscale modeling in a strong western boundary current

Using ANSYS Fluent, in this work, we have created a CFD model to characterize sub-mesoscale flows in the Florida Current over 3D space and time using field data and realistic bottom topography from an area off the East coast of Florida. The model uses a transient, pressure-based solver and Large Eddy Simulation (LES) option. LES resolves large eddies as they incorporate momentum, mass, and energy and depend on the geometry and boundary conditions. Large eddies in this context are those depending on the flow geometry. Meanwhile, small eddies are universal when modeling turbulence. The LES governing equations are formulated from time-dependent Navier-Stokes equations, filtered in either Fourier (wavenumber) space or physical space. Filtering removes eddies with scales that are too small for the grid spacing in Fluent (Ansys, I., 2018).

3.1 Straits of Florida ANSYS Fluent CFD model domain and mesh

The model domain was 1700 m in the X direction (East/West) and 852 m in the Y direction (North/South). The model domain (Fig. 2) includes the seafloor, top boundary (rigid lid), side boundaries (three inlets and one outlet), and fluid (water layer). The model included ADCP velocity data and CTD temperature data in a -200 m deep fluid region in the Z direction (vertical). A 'blank' fluid zone, ranging from ~11 to ~15 m, was created to fill the field data and the bottom topography. The bottom topography was imported and reverse-engineered from NOAA data near the mooring array.

Bottom topography data, downloaded from NOAA's Digital Elevation Model as a GeoTIFF, first had to be converted into an STL file for import to ANSYS geometry software using the DEM to 3D plugin QGIS. The STL was then imported into ANSYS SpaceClaim as a faceted body. Each side of the faceted body was skinned using reverse engineering to form a solid body. Then two boxes were added above the bottom topography. These boxes represent the fluid zone and consist of the main fluid zone (0 to -200 m) and the 'blank' zone (-200 m to bottom topography). The 'blank' zone was used to link the velocity and temperature field measurements to the boundary conditions at the non-uniform bottom topography to fill velocity and temperature values in the 'blank' zone. Once these areas were created, it was necessary to

form a single component with all three solids and share topology between them to avoid auto-generated walls at interfaces when imported into ANSYS Fluent.

The domain was then transferred to ANSYS Meshing to generate the mesh. In the field measurement zone, the cubic mesh in the Z direction matched the ADCP resolution of 4 m. The cubic mesh in the X direction was 10 m and in the Y direction 6 m. The 'blank' zone and bottom topography zones had a tetrahedral mesh to reflect the shape of the seafloor.

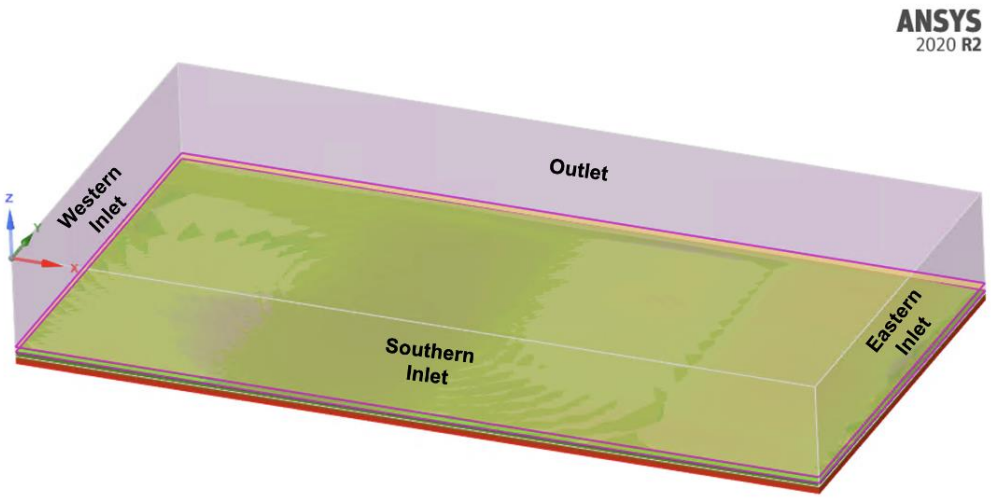

Figure 2. A model domain including main fluid zone, 'blank' fluid zone, and solid (seafloor) zone in the area of the mooring array in the Straits of Florida. The solid zone includes data imported from a NOAA digital elevation model imported into ANSYS Fluent using reverse engineering in SpaceClaim.

3.2 Model initialization with field data

Smoothed vertical velocity data for North, East, and vertical velocity components were used to make horizontal planes for each depth at the resolution of the ADCP (4 m). Profile files were used to initialize the velocity values from field data in the volume of the domain and at the boundaries of the model from field data. From the field data, text files were made containing the velocity measurements, that is, the proper number of cells for the horizontal and vertical mesh. One file was made for all velocity components of the volume initialization and individual files for each boundary. The files need to have labeled columns of x, y, and z coordinates with

corresponding values for each cell in the columns to the right. There must be header lines including [Name], name of the profile, and [Data] added according to Fluent's profile requirements for it to be read correctly. Journal files were used to read in the profile files and turn off the fixed initialization values from the model initialization and spin-up.

3.3 Numerical model setup

After loading the mesh into ANSYS Fluent, the volume profiles for velocity were read and added to the fixed values input of the fluid cell zone. The energy equation was turned on, a transient formulation and a pressure-based solver were used, and gravity was set to -9.81 m/s^2 in the Z direction. The viscous LES WALE model was used for turbulence. Water was the material in the fluid zone. The solid zone was left to default aluminum (does not interact with the fluid zone except for temperature). The seafloor boundary was set to no-slip and the top of the domain to 0 shear. Since the top of the domain is a rigid lid, this results in a complication for simulation of internal waves and tides. Due to the rigid lid at the top of the domain, internal waves and tides periodically induce backflow at the outlet. The backflow has unidentified properties, which may distort the simulation. For this reason in a subset of simulations presented in this paper we do not model internal waves and tides.

For solution methods, the Pressure-Velocity Coupling Scheme was set to simple, the gradient was set to Least Squares Cell-Based, the pressure was set to PRESTO!, momentum was set to second-order upwind, and the transient formulation was set to second-order implicit.

Volume velocity and velocity boundary conditions for the main fluid zone inlets (East, West, and South inlets – see Fig. 2) were set using interpolated ADCP field data. The inlets and volume of the 'blank' fluid zone were initially left with 0 m/s velocity because there were no ADCP data in the near bottom layer. After the initialization, the model was run to spin-up the 'blank' zone velocity field with unchanged inlet boundary conditions for 40 s. After the spin-up, the boundary conditions were set to update using the interpolated ADCP velocity data every 1-minute at the East, West, and South inlets of the main fluid zone. Figure 3a-c shows contours of the North, East, vertical velocity components after 21228 s of running the model. Figure 3d shows the velocity magnitude near the bottom topography.

After running the model for a flow time of 21228 seconds, or about six hours, we compared the model output results to the field data. Velocity profiles were exported from the outlet (North side of the domain) using CFD-Post post-processing software. A comparison of the model and ADCP (located in the center of the outlet and not involved in the boundary condition settings) profiles was conducted (Fig. 4).

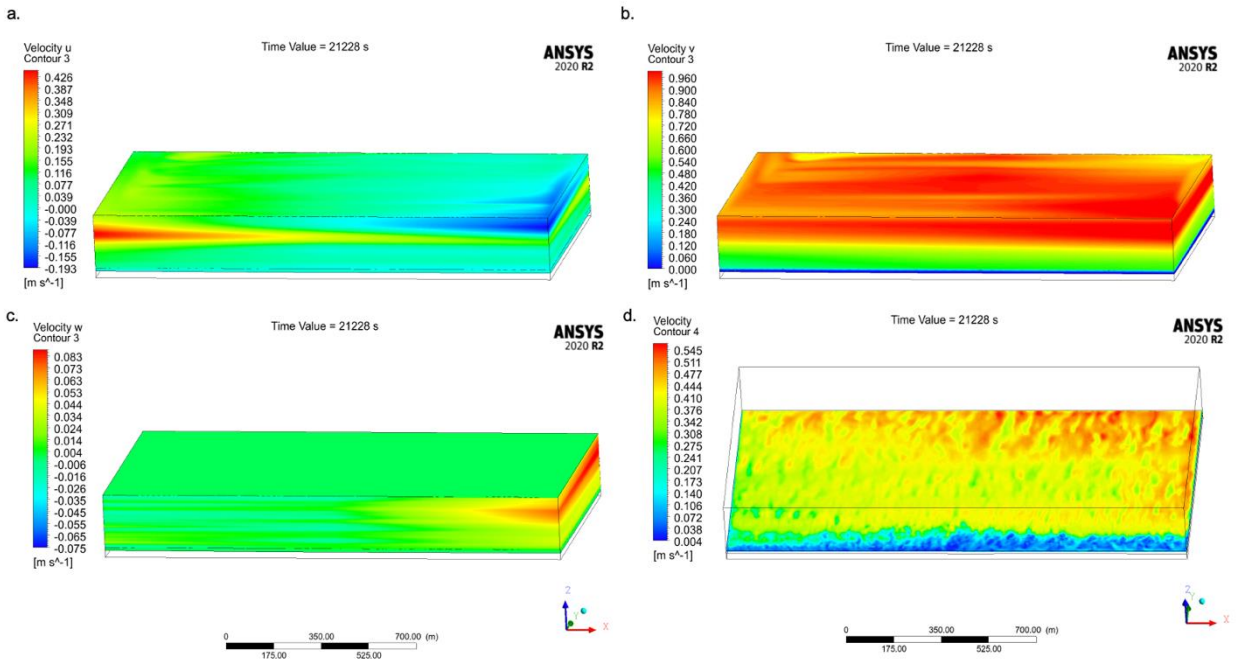

Figure 3. (a.) East velocity, (b.) North velocity, and (c.) vertical velocity contours at the East, West, North, and South boundaries and (d.) velocity magnitude near the bottom boundary after 21228 s of flow time (~6 hours).

4. Discussion

A quantitative comparison between the model and the field data was done using the control ADCP (which data not used for boundary conditions) located in the middle of the north side of the mooring array. After 6 hours of simulation, model results from the middle of the north outlet, the location of the control ADCP mooring, were exported from the model to compare to the field data. The model was verified by the comparison to the field data (Fig. 4). The comparison showed good consistency with the velocity measurements taken from the field experiment. Note that there was no field data near the seafloor because the upward looking

ADCP was providing data only starting from ~10 m above the bottom (Fig. 1b). Though this 10 m thick near bottom layer was covered by the model.

According to the results of the comparison shown in Figure 4, the model has good predictive skills in the challenging environment of a strong western boundary current and is potentially able to cover the range of ocean features from small-scales to sub-mesoscales.

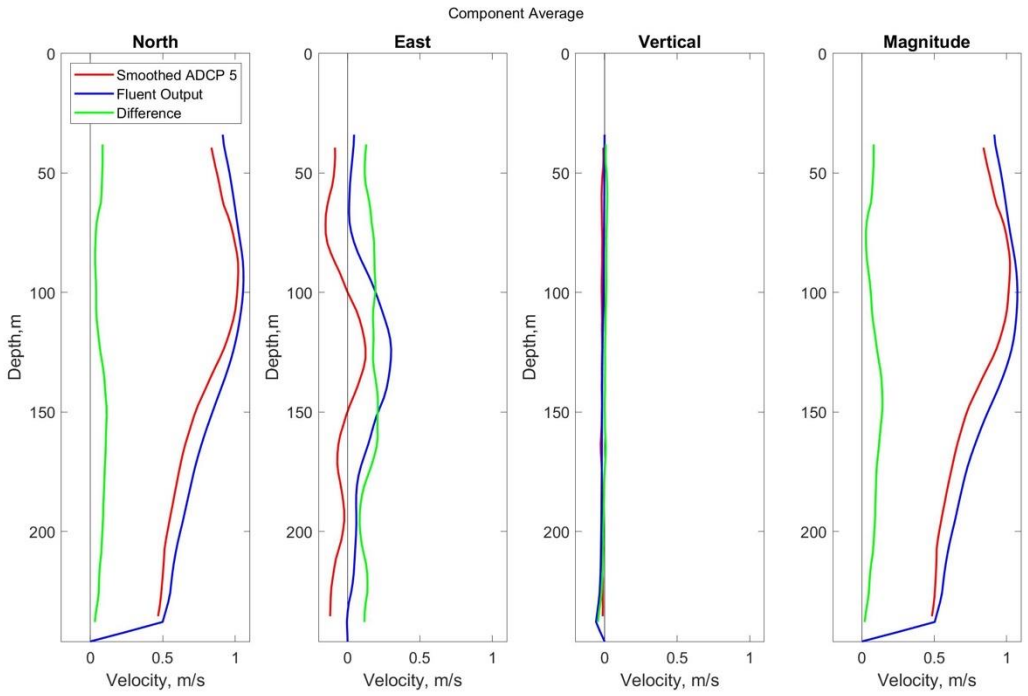

Figure 4. Comparison of North (left), East (second), vertical (third) velocity, and velocity magnitude (right) components between the ADCP field data and model output. The red line represents the smoothed ADCP data, the blue line represents the CFD model output, and the green line represents the difference between the two.

Measurements collected in the Straits of Florida were used to verify the new CFD model featuring real bottom topography. This approach combining field and modeling results may help to close the information gap between small-scale and sub-mesoscale ocean circulation in strong western boundary currents. For a more realistic simulation of the internal waves entering the experimental domain, a multiphase model including the additional (air) layer is required, which is the subject of a future upgrade.

5. Conclusions

We have proposed a modeling approach for predicting the ocean circulation in strong currents in the range from small-scales to sub-mesoscales. This approach has been verified with field data from the Straits of Florida. We anticipate this result is a starting point for sophisticated high-resolution models applicable to western boundary currents.

6. Acknowledgements

This work has been supported by the South Florida Ocean Measurement Facility (SFOMF). Any opinions, findings and conclusions or recommendations expressed in this material are those of the author(s) and do not necessarily reflect the views of the SFOMF. *The views expressed in this article are those of the author and do not necessarily reflect the official policy or position of the Department of the Navy, Department of Defense, nor the U.S. Government.*

We would like to thank Geoffrey Morrison (NSU), Brian Ettinger (NSU), Tony Bush (SFOMF), and the crew of the M/V Go America vessel and TowBoatUSA for their excellent support during the field experiments.

7. Data Availability Statement

ANSYS Fluent software used for modeling in this work is a commercial software available here: https://www.ansys.com/. Topography data was downloaded from NOAA Continuously Updated Digital Elevation Model (CUDM) Ninth Arc-Second Resolution Topographic-Bathymetric Tiles (https://coast.noaa.gov/dataviewer/#/lidar/search/where:id=8483). Data collected during field experiments are available upon reasonable request.

8. References

Ansys, I. (2018). ANSYS fluent theory guide, release 19.1. *ANSYS Inc, Canonsburg*.

Bachman, S. D., Taylor, J. R., Adams, K. A., & Hosegood, P. J. (2017). Mesoscale and submesoscale effects on mixed layer depth in the Southern Ocean. *Journal of Physical Oceanography*, *47*(9), 2173-2188.

Davis, K. A., Leichter, J. J., Hench, J. L., & Monismith, S. G. (2008). Effects of western boundary current dynamics on the internal wave field of the Southeast Florida shelf. *Journal of Geophysical Research: Oceans*, *113*(C9).

Haus, B. K., Wang, J. D., Rivera, J., Martinez-Pedraja, J., & Smith, N. (2000). Remote radar measurement of shelf currents off Key Largo, Florida, USA. *Estuarine, Coastal and Shelf Science*, *51*(5), 553-569.

Haus, B. K., Wang, J. D., Martinez-Pedraja, J., & Smith, N. (2004). Southeast Florida Shelf circulation and volume exchange, observations of km-scale variability. *Estuarine, Coastal and Shelf Science*, *59*(2), 277-294.

Koo, B., Yang, J., Yeon, S. M., & Stern, F. (2014). Reynolds and Froude number effect on the flow past an interface-piercing circular cylinder. *International Journal of Naval Architecture and Ocean Engineering*, *6*(3), 529-561.

Lee, T. N., Leaman, K., Williams, E., Berger, T., & Atkinson, L. (1995). Florida Current meanders and gyre formation in the southern Straits of Florida. *Journal of Geophysical Research: Oceans*, *100*(C5), 8607-8620.

Lee, T. N., & Williams, E. (1988). Wind-forced transport fluctuations of the Florida Current. *Journal of Physical Oceanography*, *18*(7), 937-946.

Lukas, R., & Lindstrom, E. (1991). The mixed layer of the western equatorial Pacific Ocean. *Journal of Geophysical Research: Oceans*, *96*(S01), 3343-3357.

Meinen, C. S., Baringer, M. O., & Garcia, R. F. (2010). Florida Current transport variability: An analysis of annual and longer-period signals. *Deep Sea Research Part I: Oceanographic Research Papers*, *57*(7), 835-846.

Parr, A. E. (1937). *Report on hydrographic observations at a series of anchor stations across the Straits of Florida*. Kraus Reprint.

Pillsbury, J. E. (1891). *The Gulf Stream: Methods of the investigation and results of the research* (No. 10). US Government Printing Office.

Schott, F. A., Lee, T. N., & Zantopp, R. (1988). Variability of structure and transport of the Florida Current in the period range of days to seasonal. *Journal of Physical Oceanography*, *18*(9), 1209-1230.

Simonetti, I., Cappietti, L., El Safti, H., Manfrida, G., Matthies, H., & Oumeraci, H. (2015). The use of OpenFOAM as a virtual laboratory to simulate oscillating water column wave energy converters. In *MARINE VI: proceedings of the VI International Conference on Computational Methods in Marine Engineering* (pp. 153-164). CIMNE.

Sjökvist, L., Wu, J., Ransley, E., Engström, J., Eriksson, M., & Göteman, M. (2017). Numerical models for the motion and forces of point-absorbing wave energy converters in extreme waves. *Ocean Engineering*, *145*, 1-14.

Soloviev, A. V., Luther, M. E., & Weisberg, R. H. (2003). Energetic baroclinic super-tidal oscillations on the southeast Florida shelf. *Geophysical Research Letters*, *30*(9).

Soloviev, A. V., Walker, R. J., Weisberg, R. H., & Luther, M. E. (2003). Coastal observatory investigates energetic current oscillations on southeast Florida Shelf. *Eos, Transactions American Geophysical Union*, *84*(42), 441-449.

Soloviev, A. V., Lukas, R., Donelan, M. A., Haus, B. K., & Ginis, I. (2014). The air-sea interface and surface stress under tropical cyclones. *Scientific reports*, *4*(1), 1-6.

Soloviev, A., Dean, C. W., & Fujimura, A. (2015). 3D Dynamics of Freshwater Lenses in the Near-Surface Layer of the Tropical Ocean. *Oceanography*, *28*(1), 142.

Soloviev, A. V., Lukas, R., Donelan, M. A., Haus, B. K., & Ginis, I. (2017). Is the state of the air-sea interface a factor in rapid intensification and rapid decline of tropical cyclones?. *Journal of Geophysical Research: Oceans*, *122*(12), 10174-10183.

Soloviev, A., Fujimura, A., & Matt, S. (2012). Air-sea interface in hurricane conditions. *Journal of Geophysical Research: Oceans*, *117*(C11).

Soloviev, A. V., Haus, B. K., McGauley, M. G., Dean, C. W., Ortiz-Suslow, D. G., Laxague, N. J., & Özgökmen, T. M. (2016). Surface dynamics of crude and weathered oil in the presence of dispersants: Laboratory experiment and numerical simulation. *Journal of Geophysical Research: Oceans*, *121*(5), 3502-3516.

Soloviev, A. V., Hirons, A., Maingot, C., Dean, C. W., Dodge, R. E., Yankovsky, A. E., & McCreary, J. P. (2017). Southward flow on the western flank of the Florida Current. *Deep Sea Research Part I: Oceanographic Research Papers*, *125*, 94-105.

Stern, F., Wang, Z., Yang, J., Sadat-Hosseini, H., Mousaviraad, M., Bhushan, S., Diez, M., Yoon, S.H., Wu, P.C., Yeon, M.S., Dogan, T., Kim, D.H, Volpi, S., Conger, M., Michael, T., Xing, T., Thodal, R.S., & Grenestedt, J.L. (2014, October). Recent progress in CFD for naval architecture and ocean engineering (keynote speaker). In *Proc of the 11th International Conference on Hydrodynamics (ICHD 2014)*.

Stommel, H. (1965). The Gulf Stream: A physical and dynamical description, 248 pp. *Univ. of Calif. Press, Berkeley*.

Su, Z., Wang, J., Klein, P., Thompson, A. F., & Menemenlis, D. (2018). Ocean submesoscales as a key component of the global heat budget. *Nature communications*, *9*(1), 1-8.

Thomas, L. N., Tandon, A., & Mahadevan, A. (2008). Submesoscale processes and dynamics. *Ocean modeling in an Eddying Regime*, *177*, 17-38.

Vanderplow, B., Soloviev, A. V., Dean, C. W., Haus, B. K., Lukas, R., Sami, M., & Ginis, I. (2020). Potential effect of bio-surfactants on sea spray generation in tropical cyclone conditions. *Scientific reports*, *10*(1), 1-10.

Wang, Z., Yang, J. and Stern, F. (2012) A new volume-of-fluid method with a constructed distance function on general structured grids. *Journal of Computational Physics*, 231(9), pp.3703-3722.

Windt, C., Davidson, J., & Ringwood, J. V. (2018). High-fidelity numerical modelling of ocean wave energy systems: A review of computational fluid dynamics-based numerical wave tanks. *Renewable and Sustainable Energy Reviews,93*, 610-630. doi:10.1016/j.rser.2018.05.020

Yoon, S. H., Kim, D. H., Sadat-Hosseini, H., Yang, J., & Stern, F. (2013, October). High-fidelity CFD simulation of wave run-up around vertical cylinders in monochromatic waves. In *ITTC workshop on wave run-up and vortex shedding*.

Magnetic Signature of Internal Wave Solitons from a Field Experiment in the Florida Straits

[1] John Kluge, [1] Breanna Vanderplow, [1] Cayla Dean, [2] Johanna Evans, [1] Alexander Soloviev

[1] Nova Southeastern University Halmos College of Natural Sciences and Oceanography, Dania Beach, FL, USA

[2] Naval Surface Warfare Center Carderock Division's South Florida Ocean Measurement Facility, Dania Beach, FL, USA

Abstract

Internal wave solitons are large-amplitude, localized disturbances that propagate through the ocean interior due to the interactions between density stratification and nonlinear processes. Their ability to modify density stratification and impact ocean properties and circulation makes them an important topic of study in oceanography. The electromagnetic signature produced by these solitons as they move through the Earth's magnetic field has been investigated since the 1950s and estimated using Maxwell's equations. This research aims to capture the electromagnetic signature of internal wave solitons using Acoustic Doppler Current Profilers (ADCPs) and total field magnetometers deployed in the Florida Straits. The study utilizes data processing techniques to extract the magnetic signature of passing internal waves and compares the results with the Beal and Weaver (1970) analytical model and an ANSYS Fluent Computational Fluid Dynamic Magnetohydrodynamic (CFD MHD) model. This study provides insights into the electromagnetic properties of internal wave solitons and contributes to validating existing models.

1. Introduction

Internal wave solitons are fascinating and complex oceanic disturbances that have garnered much attention from oceanographers. These types of solitons are large-amplitude, localized, and coherent disturbances that propagate through the ocean interior as a response to the interactions between density stratification and non-linear processes. Their ability to modify the ocean's density stratification, and their impacts on the distribution of properties such as temperature, salinity, and nutrients, make them an important aspect of oceanography, as noted by Apel (2002). Furthermore, their significant mixing can notably impact ocean circulation and the marine ecosystem, as Dong et al. (2015) demonstrated.

One particularly interesting aspect of internal wave solitons is their ability to produce an electromagnetic signature caused by their movement through the Earth's magnetic field. Physical oceanographers have been investigating this phenomenon since the 1950s, and have developed the theory of electromagnetic fields caused by ocean currents and surface and internal ocean waves based on Maxwell's equations (von Arx 1950; Longuet-Higgins et al. 1954; Crews and Futterman 1962; Maclure et al. 1964; Warburton and Caminiti 1964; Weaver 1965; Fraser 1966;

Larsen 1968; Beal and Weaver 1970; Sanford 1971; Podney 1975; Ochadlick 1989; Watermann and Magunia 1997; Lilley et al. 2004, Kluge et al. 2018, Kluge et al. 2022).

Podney (1975) conducted a comprehensive theoretical investigation into the electromagnetic fields generated by surface and internal waves. He aimed to provide "sensible signals" for newly developed magnetic gradiometers, which showed that "magnetic field strength above the surface is proportional to seawater speed over the ocean…; field strength decreases exponentially above the sea surface…; magnetic field gradients can provide directional information on wave spectra" (Podney 1975). The author derived and simplified the velocity profiles and magnetic signatures of internal and surface waves and evaluated the effect of different parameters on the magnetic signature through theoretical case studies.

Weaver (1965) used a simpler method to solve for the magnetic field above and below the ocean's surface than previous studies and emphasized the importance of swell, particularly long-period swell, which can significantly increase the magnetic signal even in a "slight" sea state. Through theoretical case studies, Weaver estimated the induced magnetic field per meter amplitude of surface waves as a function of altitude and depth at various wave periods. He found that even in a "slight sea-state," 20 cm amplitude waves with a 20-second period could induce a magnetic signature of 0.2 nT 100 m below the sea surface and a 0.1 nT signature 50 m above the sea surface.

Lilley et al. (2004) confirmed Weaver's findings through a real-world experiment by releasing a free-floating magnetometer off the coast of southern Australia and tracking its measurements over several days. The authors found that the period of the waves was approximately 13 seconds and typically had a signature of 5 nT trough-to-peak, consistent with Weaver's approximations. Podney (1975) explained that the electromagnetic field generated by progressive ocean waves in a horizontally stratified ocean is a combination of a transverse magnetic field and an electrostatic field, with the gradients of the magnetic field from an internal wave creating a magnetic signature based on the Josephson Effect. This magnetic signature is resolvable with modern-day magnetometers. However, ocean measurements of Earth’s magnetic field variations are challenging due to the lack of a stable sea platform, with historical magnetic records often being obtained through a magnetometer towed behind an aircraft (Weaver 1965). This method is prone to errors due to instrument instability and the consistent problem of a moving magnetometer

across a spatially varying magnetic field (Weaver 1965). Furthermore, the transverse portion of the magnetic field vanishes above the sea surface (Podney 1975). Thus, without complete and precise measurements of the magnetic signal generated by internal wave solitons, it is impossible to validate existing analytical or computational fluid dynamic (CFD) magnetohydrodynamic (MHD) models.

2. **Methods**

Data Collection and Processing

This section will provide an overview of the two instruments used in the study: Acoustic Doppler Current Profilers (ADCPs) and Geometrics G824B magnetometers. These instruments were deployed at two locations, approximately 500 meters apart, both sites containing an ADCP and magnetometer. The ADCPs velocity data were used to identify ocean phenomena, such as internal wave solitons, while the magnetometers provided data on the magnetic field. The magnetometer data had a differential method (Kluge et al. 2018, Kluge et al. 2022) applied to remove the geomagnetic external noise that both sensors would detect simultaneously.

The Acoustic Doppler Current Profilers (ADCPs) used in the study were Workhorse Quartermaster ADCPs at a frequency of 150 kHz. The Workhorse Quartermaster ADCP is a well-established oceanographic research instrument that provides high-resolution ocean currents measurements. In this study, the ADCPs were deployed in the ocean to continuously measure the velocity of ocean currents, and the data collected was used to identify solitons. The ADCPs were carefully selected for their ability to provide high-resolution measurements of ocean currents, which is critical for accurately detecting solitons in the ocean. The ADCPs were deployed on stable platforms on the seafloor looking upwards to measure 3D current velocities in our study area.

The magnetometers used in the study were Geometrics G824B Cesium magnetometers. The Geometrics G824B magnetometer is a high-precision magnetometer that provides accurate measurements of the Earth's magnetic field (Geometrics, 2015). In this study, magnetometers were deployed in the near vicinity of the ADCPs, on a stable platform, to continuously measure the total magnetic field.

Processing the data from the two instruments to extract the magnetic signature of internal wave solitons was as follows. The first step involved identifying an internal wave soliton from the ADCP data. This was achieved by analyzing the collected ADCP velocity data in WinADCP and identifying the characteristic signature of an internal wave soliton. Once an internal wave soliton was identified, the matching length of time for the two sets of magnetometer data was found. The next step involved using the differential method to remove external geomagnetic noise from the magnetometer data. The differential method involved subtracting the magnetic data collected from one magnetometer from the dataset of the other magnetometer, effectively removing any external geomagnetic noise that both sensors would detect simultaneously. This provided a cleaner and more accurate representation of the magnetic field in the ocean at the time of the passive soliton.

Analytical Model

We utilized the analytical model developed by Beal and Weaver (1970) to predict the magnetic signature of internal waves. Their model provides an approximation method for calculating the magnetic variations induced by internal ocean waves, based on a linearized magnetohydrodynamic (MHD) approximation. The approximate solutions for the magnetic field components in the upper layer ($\zeta < 0$) are

$$|h_x| = Ae^{\zeta}\{C^2\zeta^2 + S^2(1+\zeta)^2\}^{\frac{1}{2}} \quad (1)$$

$$|h_z| = Ae^{\zeta}\{S^2\zeta^2 + C^2(1-\zeta)^2\}^{\frac{1}{2}} \quad (2)$$

and the solutions of the magnetic field component below the wave interface ($\zeta > 0$) are

$$|h_x| = Ae^{-\zeta}\{C^2\zeta^2 + S^2(1-\zeta)^2\}^{\frac{1}{2}} \quad (3)$$

$$|h_z| = Ae^{-\zeta}\{S^2\zeta^2 + C^2(1+\zeta)^2\}^{\frac{1}{2}} \quad (4)$$

These magnetic field components are then used to calculate the magnetic total field

$$h_{ll} = h_x C + h_z S \quad (5)$$

The variables used in the analytical model are

$a - \ Amplitude, m$

$\sigma - \ \ Conductivity, \frac{abmho}{cm}$

$g - \ Gravity, \frac{m}{s^2}$

$\rho_1 - Density\ upper\ layer, \frac{kg}{m^3}$

$\rho_2 - Density\ lower\ layer, \frac{kg}{m^3}$

$\lambda - \ Wavelength, m$

$\theta - Wave\ propagation\ angle, degrees$

$I - \ Magnetic\ field\ inclination\ angle, degrees$

$F - Magnetic\ total\ field, G$

$D - Depth\ of\ wave\ interface, m$

$z - \ Incrementing\ depth\ from\ surface\ to\ bottom, m$

$L - Maximum\ depth\ , m$

Calculated Terms

$\alpha = \frac{\rho_2}{\rho_1}$

$m = \frac{2\pi}{\lambda}$

$A = 2\pi a \sigma F \left\{\frac{g(\alpha - 1)}{m(\alpha + 1)}\right\}^{\frac{1}{2}}$

$\zeta = m(z - D)$

$C = \cos(I) \cos(\theta)$

$S = \sin(I)$

The model is based on a simplified oceanic geometry and assumes a constant stratification, with the wave-induced velocity field approximated by a vertical sinusoidal profile. We used this model to simulate the magnetic signature of the internal waves using inputs from our

instrumentation. Additional information required for the numerical model, specifically regarding density above and below the wave interface, cannot be obtained from the sensors installed at the two test locations. To address this limitation, historical data or CTD (Conductivity, Temperature, and Depth) data from our Slocum G3 gliders were utilized during the experiment to fulfill the model's requirements.

Computational Fluid Dynamic Magnetohydrodynamic Model

ANSYS Fluent is a commercial Computational Fluid Dynamics (CFD) software that can simulate fluid flow, heat transfer, and other related phenomena. The software utilizes analytical methods to solve the governing equations that describe the behavior of fluids, such as the Navier-Stokes equations. In addition to the standard CFD capabilities, ANSYS Fluent also includes a Magnetohydrodynamics (MHD) module that simulates electromagnetic fields coupled with fluid flow (Dean 2018).

Our study used ANSYS Fluent's MHD module to simulate the behavior of internal wave solitons in the ocean (Dean 2018). Our instrumentation, including sensors and oceanographic moorings, provides data on the physical properties of the ocean, such as temperature and salinity, as well as measurements of the magnetic field. The data from the ADCP was used as inputs for the ANSYS Fluent CFD MHD model to simulate the behavior of internal wave solitons and compare the results to our field observations. By comparing the model output with the field data, we aim to validate the ANSYS Fluent CFD MHD model and gain a better understanding of the complex physical processes involved in the propagation of internal wave solitons in the ocean (Dean 2018).

3. Results

Instrumentation

In our area of study, the northern and vertical velocity components are the most informative when identifying internal wave solitons in ADCP data. The Northern velocity component (Fig. 1A) can provide useful information, as the "typical" wave pattern is often easier to identify. These types of waves often appear as a train of crests and troughs in the vertical velocity component, representing the passage of the soliton through the ocean. Solitons exhibit a distinctive pattern of positive and negative velocity values in the vertical velocity component

created by waves with alternating up and down motions (Fig. 1B). This unique pattern of velocity changes is a hallmark of internal wave solitons and a crucial factor in their identification from ADCP data. By comparing the two velocity components and looking for consistent patterns in the direction of the current, it is possible to identify the presence of internal wave solitons in ADCP data.

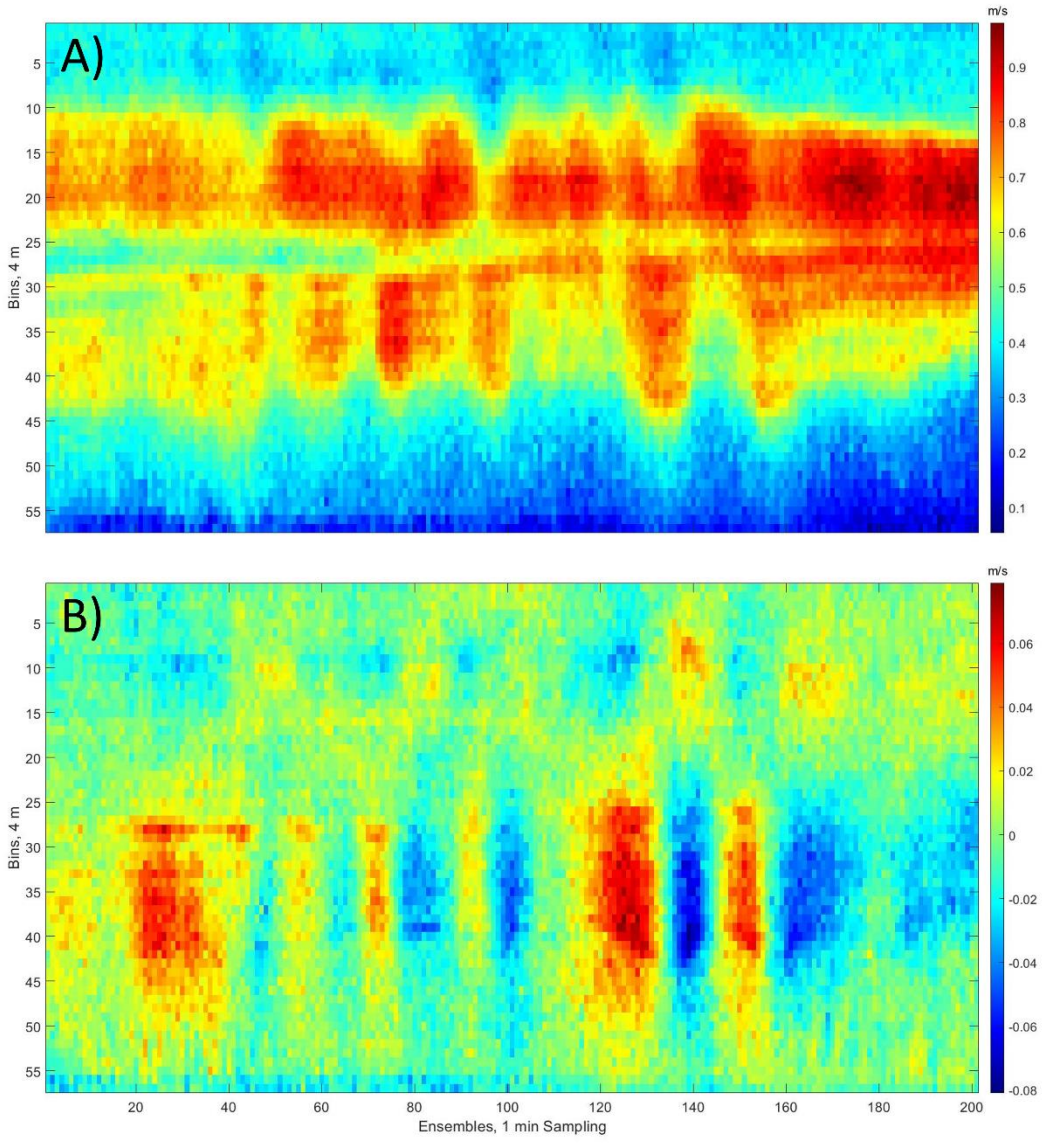

Figure 1. The characteristic signature of internal wave solitons identified from ADCP data. Figure 1A displays the Northern velocity component, and Figure 1B shows the vertical velocity component. The x-axis is the number of ensembles (measurements collected over a set time) and

the y-axis is the number of bins, which had 4-meter spacing. The color bar represents the velocity magnitude for each component.

The raw magnetic total field measurements from the magnetometers at sites 1 and 2, presented in Figure 2, were taken simultaneously with the ADCP measurements that captured the characteristic signature of internal wave soliton shown in Figure 1.

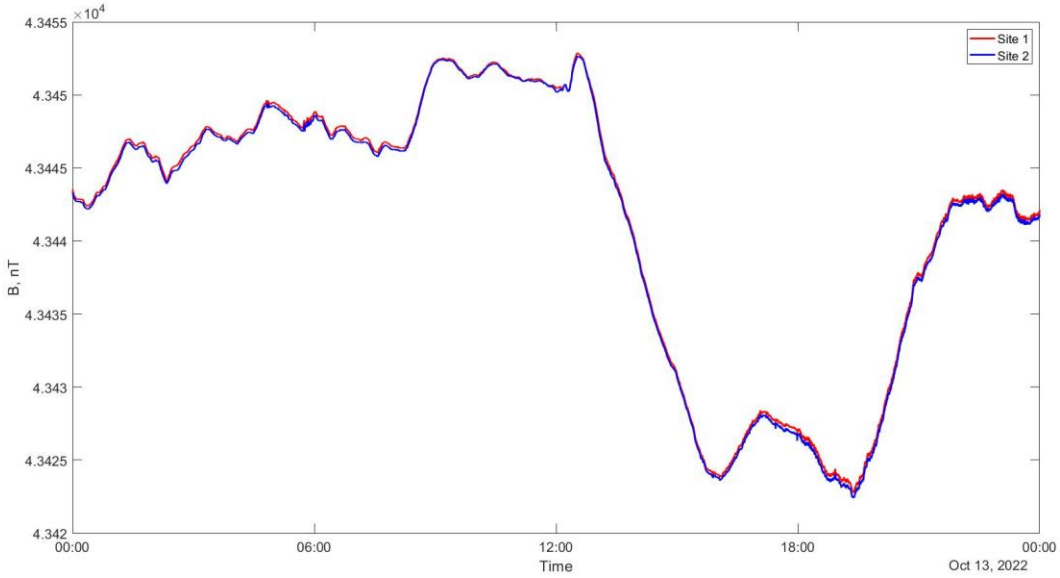

Figure 2. Raw magnetic total field measurements from the magnetometers at sites 1 and 2. The x-axis represents time, and the y-axis represents the total field measurement. The two colors are indicative of the magnetometers at each site.

Although the magnetometer data captured by the instruments deployed in the ocean at sites 1 and 2 were taken simultaneously with the ADCP measurements, the features of the internal wave solitons may not be well seen in the raw magnetometer data due to the geomagnetic noise of the Earth's magnetic field. The Earth's magnetic field is not constant and has significant variations, which can mask the small variations caused by the oceanic solitons. As a result, a differential method was applied to the data to remove any background noise both sensors would detect simultaneously, leaving behind the magnetic signature of the passing internal wave. The results of this differential method can be seen in Figure 3.

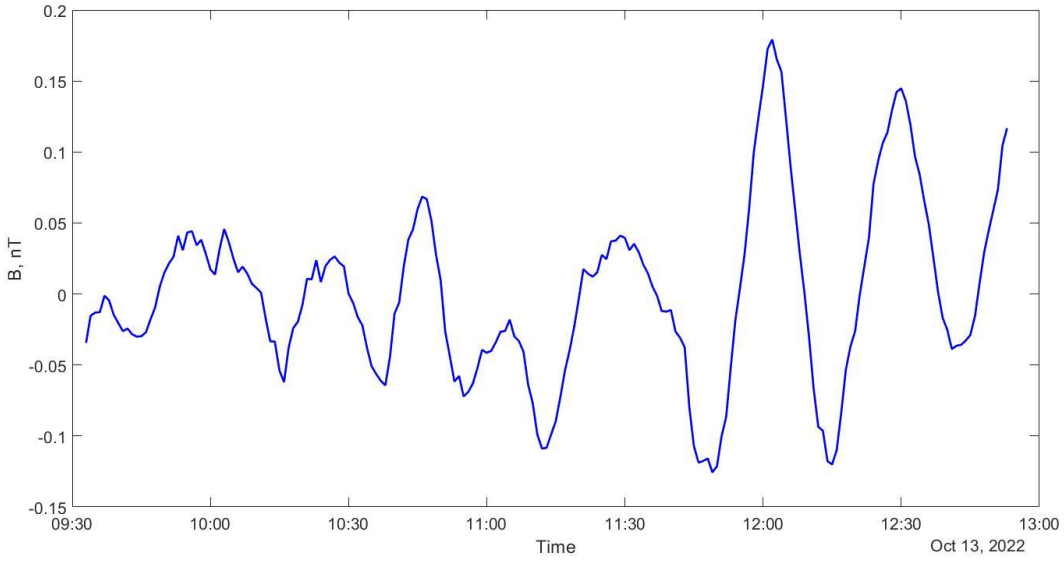

Figure 3. The differential method was applied to the centered magnetometers' raw magnetic total field measurements at sites 1 and 2.

After applying the differential method to the raw magnetometer data from sites 1 and 2, the magnetic signature of the internal wave soliton became visible. The results in Figure 23 will be used to compare the numerical and 3D CFD MHD model results. However, some other parameters used in the models must be extracted from ADCP data. One such parameter is the wavenumber, k, which can be inferred from the decay of the orbital velocities of the internal wave. The decay of orbital velocity with wavenumber is due to the dispersive nature of internal waves (Kundu & Cohen, 2004). As internal waves propagate through the ocean, their wavelength and frequency change with depth due to variations in water density and stratification. This means that longer waves with lower wavenumbers travel faster than shorter waves with higher wavenumbers (Stastna, 2022). Consequently, the orbital velocity associated with higher wavenumber waves decays more rapidly than that associated with lower wavenumber waves. The commonly used approximation for the decay of the orbital velocity amplitude with depth in a stratified fluid is:

$$V(z) = V_0 * e^{-kz} \quad (6)$$

Where V(z) is the orbital velocity at depth, V_0 is the orbital velocity at the interface of the internal wave, z is the depth, and k is the wave number (Kundu & Cohen, 2004). Since this decay

is exponential with an even increment depth, the velocity change below the internal wave's crest and trough will also decay exponentially based on wavenumber. This can be inferred from the slope of the decay shown in Figure 4.

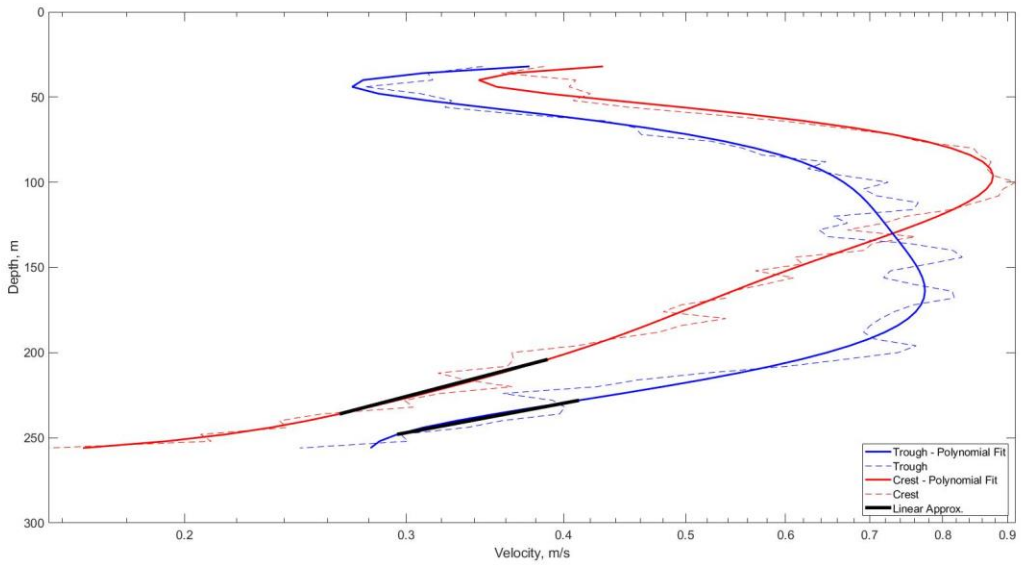

Figure 4. Wave number approximation from the vertical profile of the northern velocity component at the crest and trough the internal wave soliton. The x-axis is velocity in meters per second on a logarithmic scale and the y-axis represents depth. The blue and red lines are the velocity vertical profiles from the northern component of velocity, the trough, and crest respectively. The black lines are the linear approximations of orbital decay.

The values taken from the linear approximation in Figure 4 are shown in Table 1 as well as the resulting calculated wavenumber and wavelength.

Table 1. Table of values used to approximate wave number and the resulting wavelength from the ADCP velocity profiles.

	Ensemble	**Depth 1**	**Depth 2**	**Vel 1**	**Vel 2**	**K**	**wavelength**
Trough	134	248	228	0.2157	0.2951	0.0157	400.936
Crest	145	236	204	0.3527	0.6169	0.0175	359.624

Numerical Model

To estimate the magnetic signature of the internal wave, we assumed that the wave was moving directly north and used a rough average wavelength of 400 meters based on the data provided in Table 1. We also used local CTD data obtained from a Slocum G3 Glider to give the density of water above and below the wave interface. Subsequently, the Beal and Weaver (1970) numerical approximation model was run with these parameters, and the findings are shown in Figure 5.

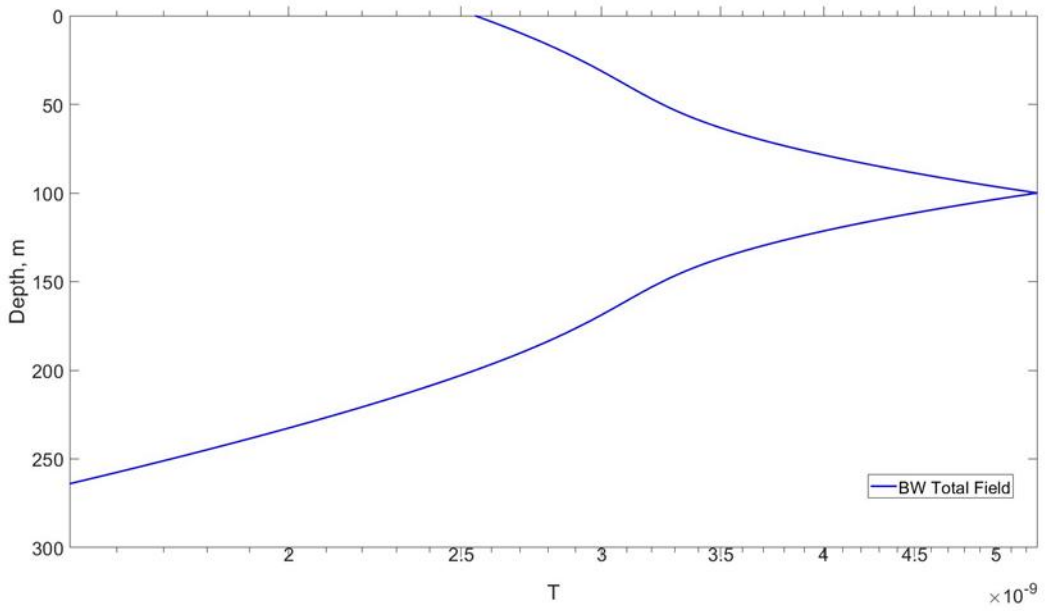

Figure 5. Magnetic total field approximation (Blue line) from the Beal and Weaver numerical model results using data from underwater instruments. The dashed black line indicates the interface depth of the internal wave.

It is evident from Figure 5 that the magnetic signature of the internal wave soliton is strongest at the interface. However, since our sensors were positioned on the seafloor, we could not directly measure the peak magnetic field strength. Based on the numerical model results, we estimated the magnetic signature of the soliton to be approximately 1.5 nT.

ANSYS Fluent CFD MHD Model

Building upon our numerical modeling results, we developed a 2D computational fluid dynamics (CFD) model in ANSYS Fluent to simulate the magnetic field response of an internal wave soliton. To ensure accurate predictions, we carefully selected the model domain size and grid resolution based on the estimated wavelength and number of ensembles. The domain length for our ANSYS Fluent CFD MHD model was calculated using the internal wave wavelength calculated in Table 1 as follows:

To find the horizontal cell size the wavelength as divided by the number of ensembles encompassing one wavelength, in this case 22 ensembles.

Cell Size = 400/22 ≈ 18.2 m

The next step was to calculate the domain length based off the 12 hours' worth of ensembles loaded into ANSYS Fluent multiplied by the cell size.

Domain length = # of ensembles loaded * Cell Size ≈ 13122 m

The domain height was set to 232 m with a 4 m cell size in the negative z direction, except for in the log layer from -228 m to -232 m, which had a 0.25 m cell size. The initial conditions for the CFD simulation were set using the velocity profiles obtained from the ADCP measurements shown in Figure 1, and the northern component of the resulting velocity field is depicted in

Figure 6.

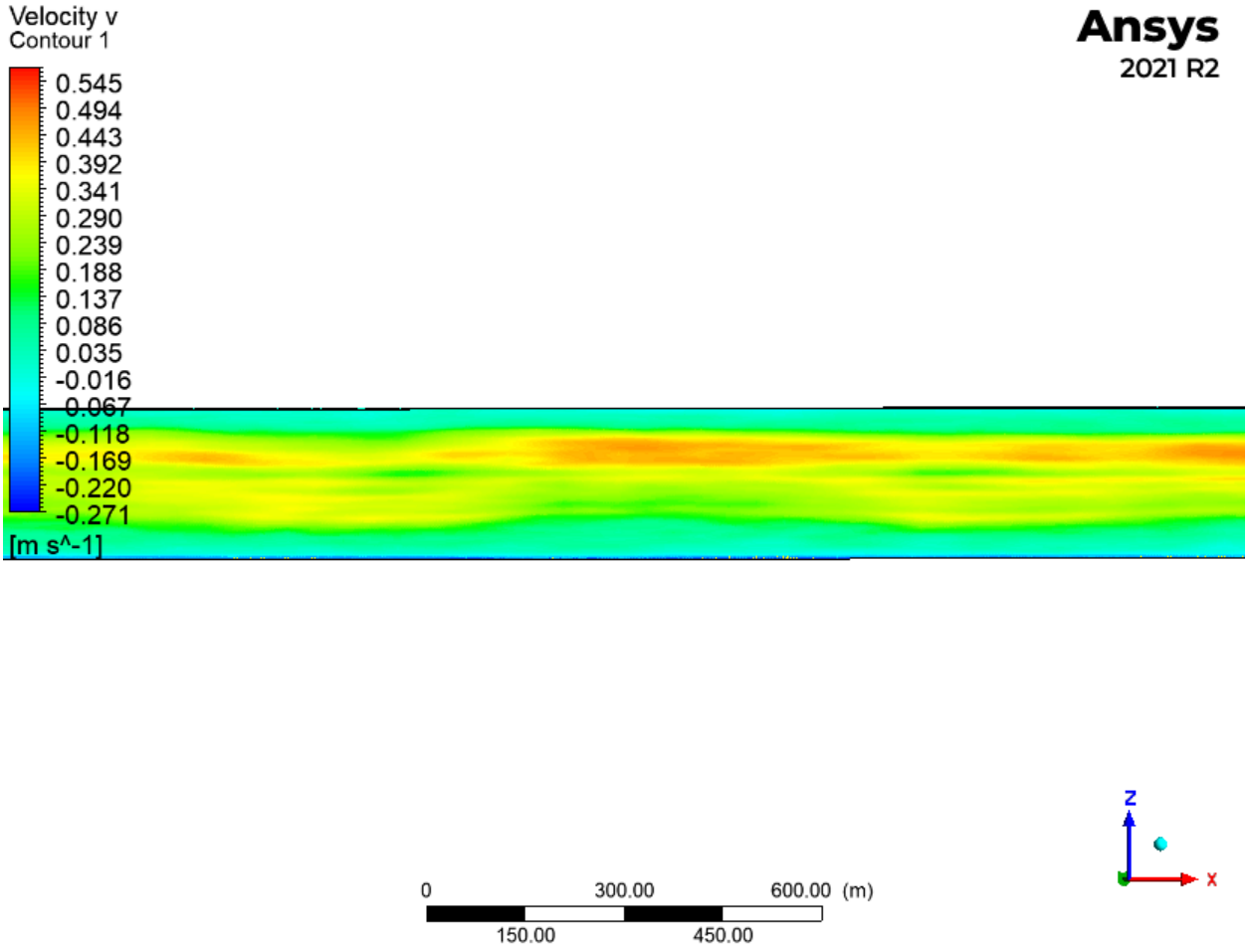

Figure 6. ANSYS Fluent model of the northern velocity component

The ANSYS Fluent model presented in Figure 6 was used to generate the modeled northern velocity component, and the resulting magnetic field was computed using the ANSYS MHD solver. The output from the MHD model is shown in Figure 7. The figure displays the spatial distribution of the magnetic field generated by the internal wave soliton, which is produced by the current flow in the modeled region. The MHD model output provides a visual representation of the magnetic field signature that corresponds to the internal wave soliton and is based on the simulated flow field.

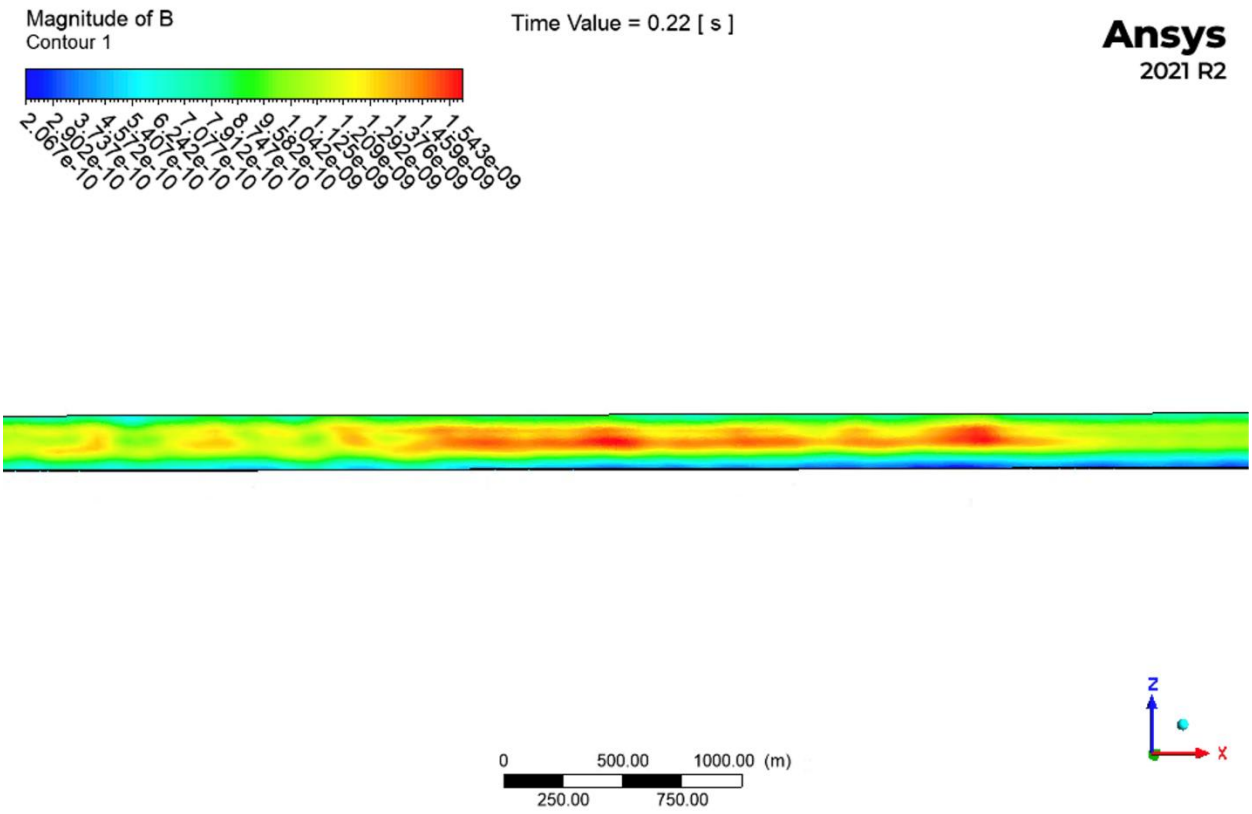

Figure 7. ANSYS MHD model output from the modeled northern velocity component.

4. Discussion

Figure 8 presents a comparison of the bin velocity data from the ADCP, and the total magnetic field time series obtained after applying the differential method. It is worth noting that the observed magnetic signal is generated by magnetometers located approximately 500 m apart, while the velocity record is obtained from a single site. Therefore, there is an offset between the peaks of the two records. Nevertheless, the comparison demonstrates a clear correspondence between the magnetic and velocity signals, indicating the successful extraction of the magnetic

signature of the internal wave soliton through the differential method.

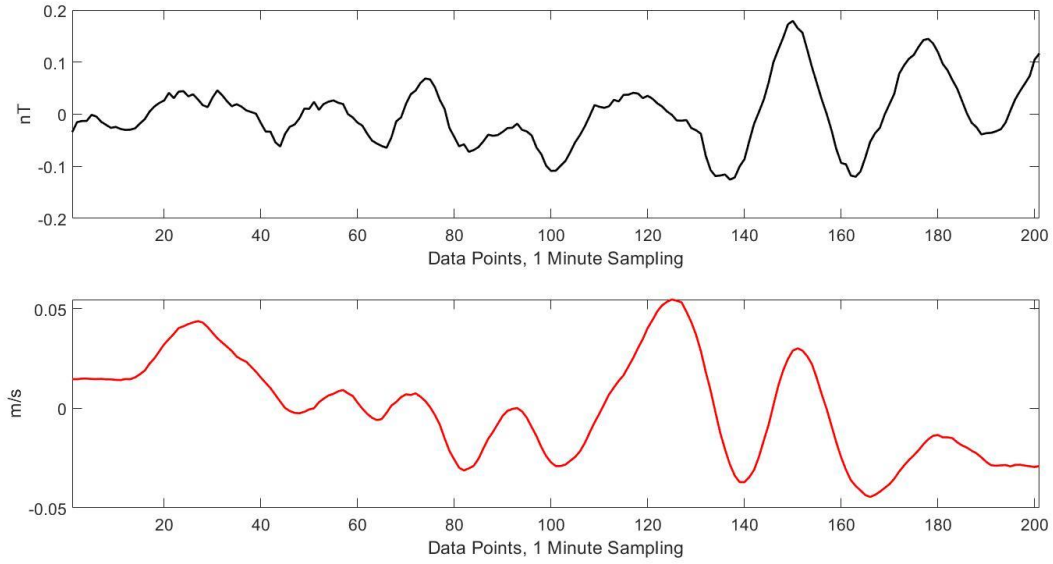

Figure 8. Comparison between the bin velocity data from an ADCP and the total magnetic field time series after the differential method was applied.

To validate our numerical model and the MHD model, we compared the field measurements to the output from each model. Figure 29 shows the comparison between the field measurements, numerical model, and ANSYS Fluent MHD model. The comparisons were made over a 12-hour period. The field measurements were obtained through the differential method applied to the magnetometer data, while the numerical and MHD models used the parameters and estimations pulled from the ADCP and historical data and the Beal and Weaver (1975) approximation.

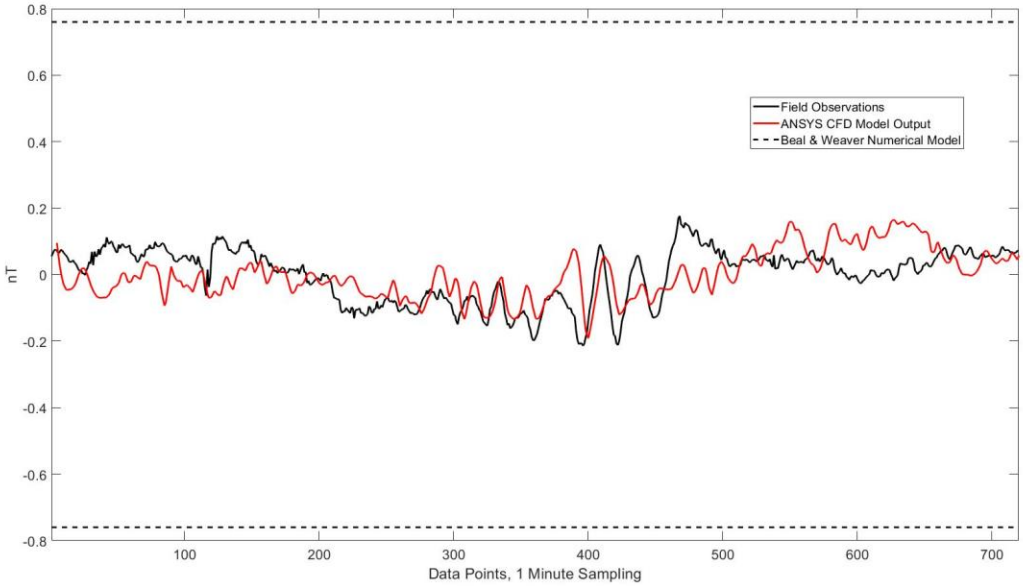

Figure 9. Comparison between field measurements, numerical model, and ANSYS Fluent Magnetohydrodynamic model.

Overall, the comparisons suggest that the CFD model can effectively recreate the magnetic signature of the internal wave soliton, shown by the comparison with field data. However, there is still room for improvement of the MHD model, particularly in areas beyond the observed soliton, which had lower levels of agreement. The numerical model proposed by Beal and Weaver (1975) had a significant discrepancy, approximately an order of magnitude higher than what was captured or recreated by either the field data or CFD MHD model, respectively. These differences with the numerical model can be attributed to the inherent assumptions made in the simplified model.

5. Conclusions

In conclusion, the magnetic signature of internal wave solitons was studied through a field experiment in the Florida Straits. We discussed the methods used for data collection and processing, including the use of our ANSYS Fluent computational fluid dynamic magnetohydrodynamic (CFD MHD) and the Beal and Weaver numerical models. The results obtained from the instrumentation and CFD MHD model showed a close match. However, the

numerical model had a significantly higher magnitude that were nearly an order of magnitude greater than both the field measurements and the CFD MHD model. This discrepancy underscores the potential limitations associated with numerical modeling when compared to real-world observations and highlights the importance of refining models to accurately capture the electromagnetic signature of internal wave solitons.

It is important to note that, although we aimed to conduct a comprehensive study, the direction of the internal wave discussed in this manuscript remained unknown. Given that the wavelength was approximately the separation of our magnetometers, coupled with our utilization of a differential method, there existed the potential for the wave to be completely out of phase, causing a doubling of our recorded signal. Conversely, if the magnetometers detected the wave simultaneously, the signal could be entirely canceled out. Nevertheless, as the magnetic signature of the internal wave remained detectable and aligned with our CFD MHD model results, we hypothesize that the wave was likely propagating in a direction that avoided both scenarios.

Acknowledgments

We would like to extend our gratitude to the Southern Florida Ocean Measurement Facility (SFOMF) for providing us with the critical data used in this work. Without their support, this study would not have been possible. Additionally, we would like to thank our team at the physical oceanography laboratory who provided historical information used to supplement the model.

References

1. Apel, J. R. (2002). Oceanic internal waves and solitons. An atlas of oceanic internal solitary waves, 1, 1-40.
2. Beal, H. T. and J. T. Weaver, 1970: Calculations of magnetic variations induced by internal ocean waves. J. Geophys. Res., 75, No. 33, 6846-6852.
3. Crews, A., & Futterman, J. (1962). Geomagnetic micropulsations due to the motion of ocean waves. Journal of Geophysical Research, 67(1), 299-306.

4. Dong, J., Zhao, W., Chen, H., Meng, Z., Shi, X., & Tian, J. (2015). Asymmetry of internal waves and its effects on the ecological environment observed in the northern South China Sea. Deep Sea Research Part I: Oceanographic Research Papers, 98, 94-101.
5. Fraser, D.C., 1966: The magnetic fields of ocean swell. Geophys. J. R. Astron. Soc., 11, 507–517.
6. Geometrics, 2015: G-824A CESIUM MAGNETOMETER Operation Manual. Geometrics, Inc revision A8, 65 pp, ftp://geom.geometrics.com/pub/mag/Manuals/824AManual_rev8.pdf.
7. Kluge J.A., A.V. Soloviev, C.W. Dean, B. Nelson, W.E. Avera, G. Valdes, B.K. Haus.2018: Magnetic Signature of Surface Waves Measured in a Laboratory Experiment, OCEANS 2018 MTS/IEEE Charleston, Charleston, SC, 2018, pp. 1-5, doi: 10.1109/OCEANS.2018.8604750.
8. Kundu, P.K., & Cohen, I.M. (2004). Fluid Mechanics. Academic Press.
9. Larsen, J. C. (1968). Electric and magnetic fields induced by deep sea tides. Geophysical Journal International, 16(1), 47-70.
10. Larsen, J.C., 1973: An introduction to electromagnetic induction in the ocean. Phys. Earth Planet. Inter., 7, 389–398.
11. Lilley,F.E.M., A. P. Hitchman, P. R. Milligan and T. Pedersen, 2004: Sea-surface observations of the magnetic signals of ocean swells. Geophys. J. Int., 159, 565–572.
12. Longuet-Higgins, M.S., Stern, M.E. & Stommel, H., 1954: The electric field induced by ocean currents and waves, with applications to the method of towed electrodes. Pap. Phys. Oceanogr. Meteor., 13, 1–37.
13. Maclure, K.C., Hafer, R.A. & Weaver, J.T., 1964: Magnetic variations produced by ocean swell. Nature, 204, 1290–1291.
14. Ochadlick, A.R., 1989: Measurements of the magnetic fluctuations associated with ocean swell compared with Weaver's theory. J. Geophys. Res., 94, 16 237–16 242.
15. Podney, W. (1975). The magnetic field above the sea surface. Reviews of Geophysics, 13(2), 221-232.
16. Podney, W., 1975: Electromagnetic fields generated by ocean waves. J. Geophys. Res., 80, 21, 2977-2990.
17. Sanford, T. B., 1971: Motionally induced electric and magnetic fields in the sea. J. Geophys. Res., 76, 15, 3476-3492.

18. Stastna, M. (2022). Internal Waves in the Ocean: Theory and Practice (Surveys and Tutorials in the Applied Mathematical Sciences #9). Springer.
19. Von Arx W. S., 1950: An electromagnetic method for measuring the velocities of ocean currents from a ship underway. Pap. Phys. Oceanogr. Meteor., 11, 3, 1-62.
20. Warburton, F., & Caminiti, R. (1964). The induced magnetic field of sea waves. Journal of Geophysical Research, 69(20), 4311-4318.
21. Watermann, J. & Magunia, A., 1997: Propagation parameters of sea surface waves inferred from observations from two closely spaced vector magnetometers. J. Geomagn. Geoelectr., 49, 709–720.
22. Weaver, J.T. (1965). Towed Proton Magnetometer Survey in the North Atlantic. Journal of Geophysical Research, 70(5), 1079-1094.